Combining Quantum Mechanics and Interatomic Potential Functions in *Ab Initio* Studies of Extended Systems

JOACHIM SAUER, MAREK SIERKA

Humboldt-Universität, Institut für Chemie, Arbeitsgruppe Quantenchemie, Jägerstrasse 10-11, D-10117 Berlin, Germany

Received 4 April 2000; accepted 25 July 2000

ABSTRACT: The errors made when large chemical systems are replaced by small models are discussed: interrupted charge transfer, missing structure constraints, neglected long-range interactions. A combined quantum mechanics (QM)–interatomic potential function (Pot) approach is described. Characteristic features of the QM-Pot approach include: (1) periodic boundary conditions, (2) consistent definition of forces in the presence of link atoms that terminate the QM cluster, (3) interatomic potential functions parametrized on *ab initio* data and accounting for polarization effects, (4) use of reaction force fields (EVB potentials) in combination with QM methods for efficient localization of transition structures in large systems, (5) implementation as a loose coupling of existing QM and Pot engines. Comparison is made with some other hybrid QM/MM methods. Applications of the combined QM-Pot method for *ab initio* modeling of the structure and reactivity of zeolite catalysts are reviewed with both protons and transition metal cations as active species. Potential functions of the ion-pair shell-model type available for such studies are compiled. The reliability of the method is checked by comparison with periodic *ab initio* studies and by examining the convergence of the results with increasing size of the QM cluster. The problems tackled are: different types of Cu^+ sites in the CuZSM-5 catalyst and their properties, acidity differences between active sites in different zeolite framework structures (energies of deprotonation, NH_3 adsorption energies), and proton mobility in acidic zeolites. The combined QM-Pot approach made possible a full *ab initio* prediction of reaction rates for an elementary process on the surface of solid catalysts and of how these rates differ between different catalysts with the same active site. © 2000 John Wiley & Sons, Inc. J Comput Chem 21: 1470–1493, 2000

Keywords: quantum mechanics; interatomic potential functions; *ab initio* studies; extended systems

Correspondence to: J. Sauer; e-mail: js@qc.ag-berlin.mpg.de
Contract/grant sponsors: Deutsche Forschungsgemeinschaft and Max–Planck-Gesellschaft

© 2000 John Wiley & Sons, Inc.

Introduction

The increasing demand for computational resources with increasing size of a chemical system is the major factor that hampers the application of *ab initio* methods to condensed phase and surface problems. Prominent examples of the latter are the determination of active site structures as well as the prediction of free energies and rates for elementary steps in enzymatic and heterogeneous catalysis. One possible solution of the problem is to limit the quantum mechanical (QM) treatment to the "active part" of the system, and to describe its environments by simple parametrized interatomic potential functions. Nowadays, such approaches are very popular and known as hybrid quantum mechanics-molecular mechanics (QM/MM) methods. The term "molecular mechanics" stresses the force field type of interatomic potential function such as MM2,[1] CFF91,[2] or CHARMM,[3] which are most useful for organic molecules and biomolecules, while inorganic solids are better described by ion-pair potential functions.[4] Therefore, we prefer the more general term combined quantum mechanics-interatomic potential function approach, QM-Pot.

The QM-Pot approach divides the energy of the whole system, S, into the QM energy of the active or inner part, I, the potential function (or MM) energy of the outer part (environment), O, and an interaction term, I-O (Fig. 1),

$$E_{\text{QM-Pot}}(S) = E_{\text{QM}}(\text{I}) + E_{\text{Pot}}(\text{O}) + E(\text{I-O}) \qquad (1)$$

The interaction term is either given by the potential function (MM method), or parts of it, the electrostatic interaction and sometimes the polarization of I by O, are described by the QM method. In the latter case, the potential due to point charges of the outer part is simply added to the core part of the Hamiltonian.

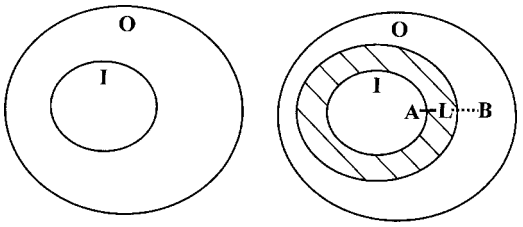

FIGURE 1. Chemical system consisting of an active (inner) part I and an outer part O. The right-hand side refers to the case in which the definition of the inner part requires the breaking of bonds, A–B. L is the link atom used to saturate the inner part for QM calculations.

In practical calculations, the three energy terms can be explicitly defined only when the two parts are not connected by chemical bonds, for example, for a solute as the inner quantum part and the solvent as the outer part.[5,6] Complications arise whenever the definition of the quantum part requires cutting bonds. The vast variety of hybrid methods or embedding schemes differs by the way this problem is handled and by the contributions of E(I-O) that are evaluated at the QM level. Most frequently the dangling bonds are saturated by so-called link atoms or capping atoms, L, and the QM calculations are performed for a cluster, C, consisting of the active part plus the link atoms, $C = \text{I} + \text{L}$. However, the complication persists that the contribution of the link atoms cannot be evaluated separately, without approximations, not even for the MM energy. From the practical point of view, the following subtraction scheme has been suggested as a solution,[7–10]

$$E_{\text{QM-Pot}}(S) = E_{\text{QM}}(C) + E_{\text{Pot}}(S) - E_{\text{Pot}}(C) \qquad (2)$$

It has the advantage that standard procedures, QM and Pot, are applied to well-defined chemical systems. If there are no link atoms, $C = \text{I}$, eq. (2) is identical with eq. (1), provided that all the interactions between the inner and the outer part, are described at the level of the interatomic potential functions, i.e., the term E(I-O) is replaced by E_{Pot}(I-O).

In the presence of link atoms, eq. (2) is only approximately valid, and may be written more accurately

$$E_{\text{QM-Pot}}(S, \text{L}) = E_{\text{QM}}(C) + E_{\text{Pot}}(S) - E_{\text{Pot}}(C) \qquad (3a)$$

with the following relation to the original definition of eq. (1):

$$E_{\text{QM-Pot}}(S) = E_{\text{QM-Pot}}(S, \text{L}) + \Delta \qquad (3b)$$

This notation stresses that the energy defined by eq. (2) depends not only on the positions of the real atoms defining the system S, but also on the positions of the link atoms.

The energy contribution of the link atoms is formally composed as follows:

$$\Delta = -E_{\text{QM}}(\text{L}) - E_{\text{QM}}(\text{L-I}) + E_{\text{Pot}}(\text{L}) + E_{\text{Pot}}(\text{L-I}) \qquad (4)$$

It will approach zero if the interatomic potential function mimics the QM potential energy surface for the terminating atoms (L) and their interaction with the inner part (L-I). Hence, the subtraction scheme defined by eq. (2) eliminates approximately the contribution from the terminating atoms that

are not part of the real system. The better the interatomic potential function fits the quantum mechanical potential energy surface (PES) for the terminating atoms the smaller is Δ. Parameters for such interatomic potentials are generally not available from empirical sources, and the use of *ab initio*-parametrized potential functions becomes mandatory. For relative energies, not the absolute value of Δ, but rather its change between products and reactants (or transition structures and reactants) is important. With increasing size of the QM cluster the interactions between the active site and the link atom region will decrease and the change of Δ will approach zero.

There is also a price to pay for the operational simplicity of eq. (2): the interatomic potential function must be also known for the active part of the system, at least it must describe the long-range interactions between the inner part and the outer part. Note that this equation also allows coupling of two quantum mechanical methods, a low-level and a high-level method as in Morokumas IMOMO scheme.[9] If $E(\text{I-O}) = E_{\text{Pot}}(\text{I-O})$, there is no direct influence of the outer part on the wave function of the cluster. Nevertheless, the electronic structure obtained from the combined QM-Pot approach is different from that of an unconstrained cluster calculation because the equilibrium structures obtained in the two optimizations are different.

There is a large number of different implementations of hybrid QM/MM methods and a broad variety of applications. A complete review exceeds the scope of the present contribution. We rather refer to the "Encyclopedia of Computational Chemistry,"[11] which includes several relevant articles,[6,12–14] to a selection of recent reviews,[15–18] and to other contributions of this special issue. Here, we present our own implementation, and point out how it differs from others. Characteristic features of QM-Pot are: (1) periodic boundary conditions, (2) a consistent definition of forces and force constants in the presence of link atoms, (3) use of *ab initio* calculations on model systems to parametrize potential functions, (4) use of potential functions that include energy terms due to the mutual polarization between the inner and the outer parts, (5) use of reaction force fields (EVB potentials) in combination with QM methods for efficient localization of transition structures in large systems, and (6) implementation as a loose coupling of existing QM and Pot engines. In the second part we review applications of the method in the field of zeolite catalysis. Special attention is paid to the evaluation of the accuracy of the QM-Pot method. Comparison is made with full QM results for periodic systems, and the convergence of the QM-Pot results with increasing size of the QM cluster is examined. At the end, we briefly review some other studies of solid-state and surface problems.

Methods

Compared to QM calculations of nonembedded clusters, the QM-Pot approach accounts for missing structure constraints and neglected long-range effects, but not for interrupted charge transfer. When link atoms are needed to terminate dangling bonds at the cluster's border, special care has to be taken when defining gradients on the atoms (or forces) for structure optimizations (or molecular dynamics runs). Analysis of QM-Pot results is facilitated by decomposition of calculated reaction energies into a QM part and a part that comprises the (long-range) corrections due to the embedding potential function. This chapter is concluded with notes on our implementation that loosely couples existing QM and Pot codes.

CLUSTER MODELS FOR EXTENDED SYSTEMS

Interrupted Charge Transfer

Formation of a chemical bond is connected with charge transfer or charge separation between the atoms forming the bond. If bonds are cut on definition of the active part, charge transfer is interrupted and the number of electrons in the active part will be different from that in the corresponding piece of the extended system. Moreover, artificial radical "dangling bond" states will show up in the gap between the occupied and virtual orbitals. Both these effects can be avoided if the cut is made not between atoms, but between bonds. Hence, a procedure is recommended that cuts atoms (e.g., C or Si) into two pseudoatoms, one belonging to the active part and one to the outer part.[19] The pseudoatom belonging to the active part consists of one electron and one hybrid orbital necessary to form a bond. A quarter of the core charge is assigned to this pseudoatom to keep the cluster neutral. The pseudoatom can be considered as "one-quarter of a C or Si atom." A pseudoatom can also be defined in such a way that the bonds connecting it with the outer neighbors are "absorbed" into the pseudoatom. That means for each bond one additional electron and one additional nuclear charge are added to the pseudoatom. In this way one arrives, for example, at a pseudocarbon atom that has

seven valence electrons, nuclear charge seven, an effective core potential, and just one free valence to make a bond to the interior of the cluster only.[20] One can either replace this pseudoatom by a real atom, in the latter case a halogen atom (see ref. 19, for example), or use a pseudopotential as done by Zhang et al.[20] This "fractional atom" scheme ensures that the charge transfer across the bonds connecting the inner part with the outer part is approximately the same as in the extended system, and that, therefore, the charge redistribution among the atoms of the inner part is approximately the same. A straightforward implementation of these ideas is the use of hybrid orbitals within semiempirical methods (see ref. 21 for a very early and ref. 22 for a recent computational sceme). In principle, it can be extended to *ab initio* methods using large basis sets. Philipp and Friesner[23] suggest the use of frozen localized bond orbitals to terminate the quantum part. These orbitals are obtained from calculations on model molecules, and will provide a standard value for the charge transfer across a given type of bond.

A more practical and widespread solution is the use of hydrogen atoms to terminate the dangling bonds of the active part. In clusters cut out of SiO_2 modifications or zeolites the terminating H atoms play the role of "a quarter of a silicon atom" (for O—H-terminated clusters) or of "one-half of an oxygen atom" (for Si—H-terminated clusters).[19] The electronegativity of H is between that of Si and O. H accepts electrons from Si (as O does), and it donates electrons to O (as Si does). This explains the success of the H-termination for clusters of silica or zeolites.

Of course, the link atoms only approximately simulate the electronic effect of the outer part (the bulk of a solid), and care must be taken that the cluster is large enough to allow for all significant charge delocalization effects. It is very important to check how the results converge with the cluster size, and how they depend on the particular choice of the cluster. This is also true for all types of combined QM-Pot (hybrid QM/MM) calculations.

There are more sophisticated approaches to allow for some charge flow between the cluster and its environment (see, e.g., the semiempirical embedding scheme of Bersuker et al.[24]). The scheme of Pisani that electronically embeds a defect site or an active site into the *ab initio* solution for the perfect periodic solid[25, 26] does not allow charge transfer between the inner part and the outer part. A correction term derived from the cluster electrochemical potential has to be added to compensate for interrupted charge transfer.[27] Interrupted charge transfer is also a key problem in recent divide-and-conquer schemes, which reduce the solution for a large system into many solutions for smaller systems (see, e.g., ref. 28).

Missing Structure Constraints

From theoretical studies on molecules in the gas phase it is known that reaction energies, vibrational frequencies, NMR chemical sifts, and many other properties crucially depend on the molecular structure, and consistent results are obtained from fully relaxed structures only. For cluster models representing interesting parts of extended systems, constrained optimization is a simple option.

The outer atoms of the cluster are fixed at "observed" atomic positions of the extended system, and the positions of the remaining internal atoms are optimized. Examples for zeolite catalysts can be found in refs. 29–31. Frequently, these positions are not accurately known (for enzymes), or are known only as an average structure of analogous crystals that do not reflect the active site properties. Adopting such atomic positions introduces artificial strain. These problems are minimized when theoretically predicted structures are used, i.e., structures found in optimizations using interatomic potential functions. However, artificial strain may also result from the fact that optimized *ab initio* structures typically show a small but systematic deviation from observed structures or from structures optimized using a different method. These problems are present in combined QM-Pot schemes that limit the optimization to the atoms of the cluster and fix all outer atoms, even if they take all long-range interactions into account, but not in schemes that relax the positions of all atoms.

Neglected Long-Range Interactions

Early, it has been suggested to make cluster models more realistic by including the long-range potential originating from the environment.[32, 33] This is done by adding the "external" potential to the one-electron part of the clusters Hamiltonian, in most cases the HF or the Kohn–Sham operator. With a few exceptions (see, e.g., ref. 34), the external potential is represented by point charges only. At a refined level, polarization of the atoms or ions in the outer part by the active part of the system is included, for example, by defining induced dipoles.[35] These are models B (Quantum Mechanical Treatment of Electrostatics) and models C (Classical Treatment of Polarization) examined in detail by Bakowies and

Thiel.[36] The appealing feature of such an approach is that the wave function or the electron density of the active part "sees" the environment. However, there are several problems: (1) when only the long-range potential is included, but not the short-range exchange-repulsion, the approach can result in artificially large charge polarizations at the cluster's border. Sometimes, the additional potential is included for an internal region of the cluster only, but not for an "insulating" region at the cluster's border.[34] (2) From technical point of view, the definition of the external potential is difficult in all cases that require link atoms. (3) The charge distribution of the active part (not expanded) and the outer part (expanded) are not treated at an equal footing. These problems seem to be more severe with *ab initio* methods than with semiempirical approaches, and are amplified if the outer atoms are included in the optimization procedure.

The QM-Pot schemes defined by eq. (2) treat the electrostatic interactions between the inner and outer parts at an equal footing, namely at the level of the interatomic potential function used. The advantage is that balanced and proven point charge or higher order models can be used, and no adjustment is necessary that is specific for the combined QM-Pot method. Even mutual polarization effects can be treated, provided that the interatomic potentials have this functional form. Basically there are three types of force fields that include polarization: induced dipoles,[35,36] shell models,[4,37] and fluctuating charge models.[38–40] The representation of the cluster region may not be as good as in a quantum mechanical description, but using the same description for both parts is more consistent.

THE LINK ATOM PROBLEM

Consistent Definition of Energies and Forces

When performing structure optimizations the link atoms must not be moved independently. They must be kept in a position in which they serve their purpose best: they have to stay on the bonds between the inner and outer part of the system that they terminate. The bond length can be either fixed or have a fixed ratio with the real bond. Hence, the link atom positions are completely fixed by constraints, and no longer independent parameters:

$$\mathbf{L}_i = \mathbf{f}_i(\mathrm{I}, \mathrm{O}) \tag{5}$$

When calculating forces on the atoms that correspond to the potential energy surface defined by eq. (2), additional contributions arise on the boundary atoms involved in the definition of the constraints (a similar derivation applies to force constants). If the bond between an atom of the active part and an atom of the outer part, A_i–B_i, $A_i \in$ I and $B_i \in$ O, is replaced by a bond between the atom A_i and a link atom, A_i–L_i, then

$$\begin{aligned}\left(\partial E_{\text{QM-Pot}}(S)/\partial \mathbf{X}_i\right)_L &= \partial E_{\text{QM-Pot}}(S, \mathrm{L})/\partial \mathbf{X}_i \\ &+ (\partial \mathbf{f}_i/\partial \mathbf{X}_i)^T\left[\partial E_{\text{QM}}(C)/\partial \mathbf{L}_i - \partial E_{\text{Pot}}(C)/\partial \mathbf{L}_i\right]\end{aligned} \tag{6}$$

with $\mathbf{X}_i = \mathbf{A}_i, \mathbf{B}_i$.

The term in parenthesis would only disappear if Δ, cf. eq. (4), were exactly zero. For brevity, in the following we will drop the "L" in the symbol for the QM-Pot energy, $E_{\text{QM-Pot}}(S, \mathrm{L})$, except in a few places.

For the atoms not involved in the link atom definition we get

$$\begin{aligned}\partial E_{\text{QM-Pot}}(S)/\partial \mathbf{I}_i = \partial E_{\text{QM}}(C)/\partial \mathbf{I}_i + \partial E_{\text{Pot}}(S)/\partial \mathbf{I}_i \\ - \partial E_{\text{Pot}}(C)/\partial \mathbf{I}_i\end{aligned} \tag{7}$$

$$\partial E_{\text{QM-Pot}}(S)/\partial \mathbf{O}_i = \partial E_{\text{Pot}}(S)/\partial \mathbf{O}_i. \tag{8}$$

The constraints can be any function of the positions of the atoms in the I and O parts. We use a simple form in terms of Cartesian coordinates,

$$\mathbf{L}_i = \mathbf{A}_i + g_i(\mathbf{B}_i - \mathbf{A}_i), \tag{9}$$

where g_i is a ratio between the A_i–L_i and A_i–B_i distances,

$$g_i = |A_iL_i|/|A_iB_i| = \text{const}\,/|A_iB_i|. \tag{10}$$

It leads to the following expression for the gradients on the A_i and B_i atoms:

$$\begin{aligned}\left(\frac{\partial E_{\text{QM-Pot}}(S)}{\partial \mathbf{A}_i}\right)_L &= \frac{\partial E_{\text{QM-Pot}}(S)}{\partial \mathbf{A}_i} + \left(\mathbf{1} + g_i\left(\mathbf{n}_i\mathbf{n}_i^T - \mathbf{1}\right)\right) \\ &\times \left(\frac{\partial E_{\text{QM}}(C)}{\partial \mathbf{L}_i} - \frac{\partial E_{\text{Pot}}(C)}{\partial \mathbf{L}_i}\right)\end{aligned} \tag{11}$$

$$\begin{aligned}\left(\frac{\partial E_{\text{QM-Pot}}(S)}{\partial \mathbf{B}_i}\right)_L &= \frac{\partial E_{\text{QM-Pot}}(S)}{\partial \mathbf{B}_i} - g_i\left(\mathbf{n}_i\mathbf{n}_i^T - \mathbf{1}\right) \\ &\times \left(\frac{\partial E_{\text{QM}}(C)}{\partial \mathbf{L}_i} - \frac{\partial E_{\text{Pot}}(C)}{\partial \mathbf{L}_i}\right)\end{aligned} \tag{12}$$

The matrix $\mathbf{1}$ is the 3×3 unit matrix and $\mathbf{n}_i$ is a unit vector along the A_i–B_i bond pointing towards B_i. Similar expressions can be derived for the second derivatives of the QM-Pot energy.

At this point our QM-Pot method differs from the *recent* version of Morokuma's ONIOM approach, which defines g_i as a constant.[41] This leads to a particularly simple form of the modified derivatives, where the $\mathbf{n}_i\mathbf{n}_i^T$ matrix is skipped in eqs. (11) and (12).

We define the constraints such that the link atoms are at a constant distance from A_i along the A_i–B_i bond. With this definition the QM-Pot gradient on the A_i–B_i bond distance is the same as the Pot gradient on this bond in the real system S. In contrast, due to the constraints used in the ONIOM scheme the force on the A_i–B_i bond has additional contributions from link atoms. Note also that earlier implementations of the IMOMM, IMOMO, and ONIOM methods defined the constraints on link atoms in internal coordinates.[9, 12, 42] This definition is equivalent to the one in Cartesian coordinates [eq. (9)], but requires a definition of internal coordinates, for example, by setting up a Z-matrix, which is not always straightforward. The original IMOMM method[42] was not defined by the subtraction scheme [eq. (2)]. Rather "double counting" of terms was avoided by crossing out those terms from the MM expression for S that were already accounted for by the QM cluster calculations. The subtraction scheme for IMOMM, eq. (2), was introduced together with the IMOMO method.[9]

Note that the gradients derived from eqs. (7), (8), (11), and (12) fulfill all the requirements that follow from the translational and rotational invariance[43] of $E_{\text{QM-Pot}}(S)$ as defined by eq. (2) under constraints such as given by eq. (9).

Weiners Molecular Dynamics Approach

Weiner et al.[44] developed a molecular dynamics method with combined quantum (AM1 Hamiltonian) and empirical potentials (modified Stillinger–Weber potential parametrized on QM data). They saturate the quantum part by link atoms, which, as in our QM-Pot method, are constraint to stay on the A–B bonds connecting the inner and the outer parts. The parameter g in eq. (10) is a constant obtained as the ratio of standard values for A–L and A–B bond distances, for exmple, r(Si—H)/r(Si—Si) for cluster models of solid silicon. (Note that Weiner et al.[44] use a different terminology and they call the A and B atoms link atoms.) Their scheme is defined in terms of forces. For the atoms of the inner part not involved in the link atom definition, I $\neq$ A, forces are taken from the QM cluster calculation

$$\partial E_{\text{Weiner}}(S)/\partial \mathbf{I}_i = \partial E_{\text{QM}}(C)/\partial \mathbf{I}_i. \tag{13}$$

Forces on the A atoms (to which the link atoms are attached) *are calculated from the potential function only*,

$$\partial E_{\text{Weiner}}(S)/\partial \mathbf{A}_i = \partial E_{\text{Pot}}(S)/\partial \mathbf{A}_i, \tag{14}$$

as are the forces on the atoms of the outer part, including the B atoms

$$\partial E_{\text{Weiner}}(S)/\partial \mathbf{O}_i = \partial E_{\text{Pot}}(S)/\partial \mathbf{O}_i. \tag{15}$$

To see which approximations are involved in such a definition we have to define the total energy belonging to this scheme (which is not done by the original authors):

$$E_{\text{Weiner}}(S, \text{L}) = E_{\text{QM}}(C) + E_{\text{Pot}}(\text{O}) + E_{\text{Pot}}(\text{I-O}). \tag{16}$$

Note that the last two terms are not evaluated separately, but the potential function is used for calculations on the whole system:

$$E_{\text{Pot}}(S) = E_{\text{Pot}}(\text{I}) + E_{\text{Pot}}(\text{O}) + E_{\text{Pot}}(\text{I-O}). \tag{17}$$

The total energy defined by eq. (16) differs from the definition of eq. (2),

$$E_{\text{QM-Pot}}(S) = E_{\text{Weiner}}(S, \text{L}) + \Delta_{\text{Weiner}} \tag{18}$$

with

$$\Delta_{\text{Weiner}} = E_{\text{QM}}(\text{I}) - E_{\text{QM}}(C) = -E_{\text{QM}}(\text{L}) - E_{\text{QM}}(\text{L-I}) \tag{19}$$

Comparison with eq. (4) reveals that the contributions from the link atoms are not approximately compensated as in the subtraction schemes, eq. (2).

Differentiating eq. (16), we find that the force definitions of eqs. (13)–(15) only hold if:

$$I \neq A \qquad \partial E_{\text{Pot}}(\text{I-O})/\partial \mathbf{I}_i = 0 \tag{20}$$

$$A \qquad \partial E_{\text{QM}}(C)/\partial \mathbf{A}_i = \partial E_{\text{Pot}}(\text{I})/\partial \mathbf{A}_i. \tag{21}$$

The derivative of the total energy with respect to the link atom positions is

$$\partial E_{\text{Weiner}}(S)/\partial \mathbf{L}_i = \partial E_{\text{QM}}(C)/\partial \mathbf{L}_i \tag{22}$$

As shown by eqs. (11) and (12), this derivative makes additional contributions to the forces on the A_i and B_i atoms, because constraints apply to the link atom positions. Neglecting them is an additional approximation.

These inconsistencies cannot be rectified by assuming that another implicit definition of the total energy, for example, that given by eq. (1) applies,

$$E_{\text{Weiner-1}}(S) = E_{\text{QM}}(\text{I}) + E_{\text{Pot}}(\text{O}) + E_{\text{Pot}}(\text{I-O}). \tag{23}$$

With this assumption,

$$\partial E(S)_{\text{Weiner-1}}/\partial \mathbf{L}_i = 0, \tag{24}$$

but the above force definitions, eqs. (13)–(15), follow only from eq. (23) if it is assumed that

$$I \neq A \qquad \partial E_{\text{QM}}(\text{L-I})/\partial \mathbf{I}_i = \partial E_{\text{Pot}}(\text{I-O})/\partial \mathbf{I}_i \tag{25}$$

$$A \qquad \partial E_{\text{QM}}(\text{I})/\partial \mathbf{A}_i = \partial E_{\text{Pot}}(\text{I})/\partial \mathbf{A}_i. \tag{26}$$

These conditions are only fulfilled if the potential function perfectly mimics the QM potential energy surface in the inner region and if the QM contributions of the L-I interactions to the forces on the atoms of the inner region are the same as the interatomic potential function contributions from the outer region atoms. Potential functions carefully parametrized on QM data may approximately serve this need.

The authors are aware of the approximate nature of their forces:[44] "in the present implementation of combined dynamics ... forces exerted on" A atoms "due to atoms on the interior of the quantum cluster," $I \neq A$, "are not met by precisely equal and opposite forces exerted by" A atoms "on the interior atoms. Such an inequality can induce artificial motions in an MD run which can be eliminated by removing the linear and angular momenta of the system as a whole in every time step."

We have discussed this method in some detail, because it highlights the importance of a consistent definition of forces.

SIMOMM Method

Shoemaker et al.[45] have modified the original IMOMM[42] method for use in surface cluster studies. Their working equation for the total energy of the combined system is the same as we have assumed for the Weiner method, eq. (16).

$$E_{\mathrm{SIMOMM}}(S, \mathrm{L}) = E_{\mathrm{QM}}(C) + E_{\mathrm{Pot}}(S) - E_{\mathrm{Pot}}(\mathrm{I}). \quad (27)$$

The potential part is calculated by crossing out terms from the expression for the whole system that apply to the inner part only.

$$E_{\mathrm{Pot}}(\mathrm{O}) + E_{\mathrm{Pot}}(\mathrm{I\text{-}O}) = E_{\mathrm{Pot}}(S) - E_{\mathrm{Pot}}(\mathrm{I}) \quad (28)$$

Equations (18) and (19) hold accordingly, i.e., the SIMOMM method does not approximately remove the contribution of the link atoms that are not part of the real system.

The main idea behind the SIMOMM method is to lift the constraints on link atoms and let them move according to the forces obtained from eq. (27).

$$\partial E_{\mathrm{SIMOMM}}(S)/\partial \mathbf{L}_i = \partial E_{\mathrm{QM}}(C)/\partial \mathbf{L}_i. \quad (29)$$

The forces on the I and O atoms are obtained by differentiating eq. (27).

$$\partial E_{\mathrm{SIMOMM}}(S)/\partial \mathbf{I}_i = \partial E_{\mathrm{QM}}(C)/\partial \mathbf{I}_i + \partial E_{\mathrm{Pot}}(\mathrm{I\text{-}O})/\partial \mathbf{I}_i \quad (30)$$

$$\partial E_{\mathrm{SIMOMM}}(S)/\partial \mathbf{O}_i = \partial E_{\mathrm{Pot}}(S)/\partial \mathbf{O}_i \quad (31)$$

Because no constraints apply, these are well-defined forces that unlike the forces of the Weiner scheme fulfill the requirements that follow from the rotational and translational invariance of eq. (27), and there would be no problem with using them in an MD mode.

The unconstrained motions of the link atoms will be no problem, as long as it can be expected that the direction of the A–L bond stays close to the direction of the A–B bond. For silicon surfaces and reactions on it for which the method was designed, this is very likely to be the case, as Si—Si—Si and Si—Si—H bond angles are all close to the tetrahedral angle. However, with systems such as silica and zeolites problems may arise from the fact that Si—O—Si bond angles are around 145°, while Si—O—H angles are around 115°.

One of the motivations for lifting the constraints was that definitions in terms of internal coordinates are not practical for solids. We have shown above that constraints can well be defined in Cartesian coordinates. Moreover, by using the subtraction scheme, eq. (2), instead of the "elimination" or "crossing out" scheme, eq. (27), the link atom contributions to the potential energy surface can be approximately removed.

DECOMPOSITION OF REACTION ENERGIES

For a reaction,

$$R \rightarrow P,$$

the energy can be expressed as

$$\Delta E_{\mathrm{QM\text{-}Pot}} = \Delta E_{\mathrm{QM}} + \Delta E_{\mathrm{Pot}} \quad (32)$$

with

$$\Delta E_{\mathrm{QM}} = E_{\mathrm{QM}}(C_P) - E_{\mathrm{QM}}(C_R) \quad (33)$$

and

$$\Delta E_{\mathrm{Pot}} = E_{\mathrm{Pot}}(S_P) - E_{\mathrm{Pot}}(S_R) - E_{\mathrm{Pot}}(C_P) + E_{\mathrm{Pot}}(C_R) \quad (34)$$

The subscripts R and P refer to the reactants and products, respectively.

To see the physical meaning of ΔE_{Pot}, we rewrite eq. (34) as follows ($S = \mathrm{I} + \mathrm{O}$, $C = \mathrm{I} + \mathrm{L}$):[46]

$$\Delta E_{\mathrm{Pot}} = \Delta E_{\mathrm{Pot}}(\mathrm{O}) + \Delta E_{\mathrm{Pot}}(\mathrm{I\text{-}O}) - \Delta E_{\mathrm{Pot}}(\mathrm{L}) - \Delta E_{\mathrm{Pot}}(\mathrm{L\text{-}I}) \quad (35)$$

If the cluster is chosen such that the reaction changes the internal part of the system only, the structures of the outer region and the link atom region are the same, and both

$$\Delta E_{\mathrm{Pot}}(\mathrm{O}) = E_{\mathrm{Pot}}(\mathrm{O}_P) - E_{\mathrm{Pot}}(\mathrm{O}_R) \quad (36a)$$

and

$$\Delta E_{\text{Pot}}(\text{L}) = E_{\text{Pot}}(\text{L}_P) - E_{\text{Pot}}(\text{L}_R) \tag{36b}$$

vanish. We obtain:

$$\Delta E_{\text{Pot}} = \Delta E_{\text{Pot}}(\text{I-O}) - \Delta E_{\text{Pot}}(\text{L-I}) \tag{37}$$

If the cluster is large enough that all short-range terms of the interatomic potentials vanish between the reaction site and the cluster boundary, only long-range terms persist in eq. (37) and

$$\Delta E_{\text{Pot}} \approx \Delta E_{\text{L}_R} \tag{38}$$

Hence,

$$\Delta E_{\text{QM-Pot}} \approx \Delta E_{\text{QM}/\!/\text{QM-Pot}} + \Delta E_{\text{L}_R/\!/\text{QM-Pot}} \tag{39}$$

Use has been made of the notation "//QM-Pot," which means "at the structure obtained by the combined QM-Pot method." This way of writing eq. (39) reflects that the QM-Pot approach has two effects: (1) the quantum mechanical contribution to the reaction energy is calculated at structures of the reactants and products that have been obtained by the combined QM/MM approach (limited relaxation compared to free space optimized clusters). This makes the QM result within the QM-Pot scheme different from the QM result for a gas phase cluster because the structure is different. (2) The interatomic potential functions applied to the interaction between inner and outer region provide a long-range correction to the reaction energy calculated. Provided that the type of potential function used accounts for polarization effects as, for example, the shell-model potential does, energy contributions due to mutual polarization effects between the inner and the outer regions are included.

AB INITIO-DERIVED POTENTIAL FUNCTIONS

In this section we will describe the potential functions that our group has derived from *ab initio* data and that have been used in the combined QM-Pot studies on zeolites described below. The beginning was a large set of Hartree–Fock data for cluster models of silica and zeolites (energies, gradients for structures distorted from equilibrium and force constants), which were used to parametrize both "consistent force field" potential functions[2, 47, 48] and ion-pair shell-model potential functions.[4, 49, 50] Table I summarizes the potentials available for different types of zeolite catalysts.[8, 37, 51–57] A more complete review of interatomic potential functions proposed for zeolites and related microporous and mesoporous systems is given in refs. 58–60.

Force Fields

Force fields are interatomic potential functions whose analytical form originates from a Taylor expansion of the potential energy V of a polyatomic system around its equilibrium structure R^0 using internal coordinates R_i such as bond distances, bond angles, and out-of-plane angles:

$$\begin{aligned} V = V_0 &+ (1/2)\Sigma_i F_{ii}\left(R_i - R_i^0\right)^2 \\ &+ (1/6)\Sigma_{iii} F_{iii}\left(R_i - R_i^0\right)^3 \\ &+ (1/24)\Sigma_{iiii} F_{iiii}\left(R_i - R_i^0\right)^4 \\ &+ (1/2)\Sigma_{ij} F_{ij}\left(R_i - R_i^0\right)\left(R_j - R_j^0\right) \\ &+ V^{\text{torsion}} + V^{\text{angle-torsion-angle}} + V^{\text{nonbond}} \end{aligned} \tag{40}$$

TABLE I.
***Ab Initio* Parametrized Interatomic Potential Functions for Zeolite Catalysts and Related Materials.**

Functional Form	*Ab Initio* Method	Parameters Available for	Refs.
Consistent force field	HF/T(O)DZP	SiO_2, H—$AlO_2(SiO_2)_n$	8, 51, 52
Ion-pair shell model	HF/T(O)DZP	SiO_2, H—$AlO_2(SiO_2)_n$	55
Ion-pair shell model	HF/T(O)DZP	$H_3N{\cdot}H$—$AlO_2(SiO_2)_n$ $NH_4^+(AlO_2^-)(SiO_2)_n$	63
Ion-pair shell model	DFT/T(O)DZP	SiO_2, H—$AlO_2(SiO_2)_n$ CuI—$AlO_2(SiO_2)_n$	37 54
Ion-pair shell model (EVB)	DFT/T(O)DZP	H—$AlO_2(SiO_2)_n$ O—H—O proton jump	56
Ion-pair shell model		AlO_2PO_2, H—$SiO_2(AlO_2)_n(PO_2)_{n-1}$	53
Ion-pair shell model	HF/SVP	SiO_2, Ti-subst. SiO_2 Si—OH and Ti—OH groups $(H_2O)_n{\cdot}TiO_{4/2}$	57

F_{ii}, F_{iii}, and F_{iiii} have the formal meaning of harmonic, cubic, and quartic diagonal force constants, respectively. Nondiagonal terms ($i \neq j$) represent harmonic couplings. Special functional forms are used for the torsional angles and the angle-torsion-angle coupling term.

$$V^{\text{torsion}} = \Sigma_i\left[V_i^{(1)}(1-\cos\phi_i) + V_i^{(2)}(1-\cos 2\phi_i) + V_i^{(3)}(1-\cos 3\phi_i)\right] \quad (41)$$

$$V^{\text{angle-torsion-angle}} = \Sigma_{ijk}F_{ijk}\left(R_i - R_i^0\right)\cos\phi_j\left(R_k - R_k^0\right) \quad (42)$$

Equation (40) can be rewritten grouping together all contributions of a particular type of internal coordinates:

$$V = V_0 + V^{\text{bonds}} + V^{\text{angles}} + V^{\text{torsion}} + V^{\text{out-of-plane}} + V^{\text{bond-bond}} + V^{\text{angle-angle}} + V^{\text{bond-angle}} + V^{\text{angle-torsion-angle}} + V^{\text{nonbond}} \quad (43)$$

The latter equation includes a so-called nonbond term that is part of almost all force fields. It is an explicit atom–atom pair term for the interactions between atoms, which are separated in a molecule by at least three or four bonds:

$$V^{\text{nonbond}} = \Sigma_{i>j}^{\text{nonbond}}\left(V_{SR}(i,j) + q_iq_j/r_{ij}\right) \quad (44)$$

This is not consistent with the Taylor expansion idea, but avoids the need of higher order coupling terms. The short-range part, V_{SR}, in the case of the consistent force field CFF91 has the form:[2]

$$V_{SR}(i,j) = \varepsilon_{ij}\left[2(r_{ij}^*/r_{ij})^9 - 3(r_{ij}^*/r_{ij})^6\right] \quad (45)$$

The van der Waals well depth and radius, ε_{ij} and r_{ij}^*, respectively, are obtained from atom type parameters ε_i and r_i^*. The effective atomic charges q_i are obtained from bond increments, which ensures proper charge balance in the whole system:

$$q_i = \sum_j \delta_j \quad (46)$$

The sum runs over all bonds j originating at atom i.

A force field is defined for polyatomic systems with well-defined bonds. It is potentially capable of describing all degrees of freedom of a zeolite catalyst loaded with sorbate molecules. The internal flexibility of both the zeolite and the adsorbed molecule could be accounted for, and the nonbond term would provide a description of the intermolecular interaction between the molecule and the zeolite surface. However, the nonbond parameters derived with the purpose of a good description of the zeolite structure itself or the structure of the adsorbed molecule may not be the best choice for the description of zeolite–sorbate interactions.

The disadvantage of the force field form is the large number of parameters. The analytical form of a Taylor expansion creates problems if internal coordinates can assume a broad range of values about the reference value. In this case the terms $(R_i - R_i^0)$ become large, and coupling terms become also large. An example is the Al—O bond in the zeolitic SiO(H)Al Brønsted sites.[52] In principle, the Taylor expansion could still describe this situation, but only if diagonal and coupling terms to very high order would be included. This is not practical, because the number of parameters would become very large.

Parametrization is made by a best fit to either empirical data or data obtained by quantum mechanical calculations. Because all (or most) parameters are adjusted at the same time, and because the same parameters are used for similar bonding situations in different systems, the parameters obtained do not have the physical meaning that the functional form chosen may imply. For example, the parameters used for the nonbond term in a force field may differ from the parameters of the same expression used for describing intermolecular interactions. The reason is that in the former case part of the atom–atom interaction is already accounted for by the force constants. A frequently discussed question is the choice of charges. It should be understood that point charges defined in any interatomic potential function are parameters that have a meaning only in the context of this particular multiparameter function. In particular, such charge parameters must not be confused with the charge distributions inferred from general bonding considerations. The ion-pair shell-model potentials for zeolites that proved very successful both with empirically derived and *ab initio*-based parameter sets all assume full formal charges. In contrast, the atomic charges used in the CFF-type force field of zeolites are much smaller fractional charges. They are even smaller than charges needed for describing intermolecular interactions between the zeolite framework and an adsorbed molecule. In short, charges used in any form of interatomic force field are model dependent parameters.

Ion-Pair Potentials

Simple interatomic potentials for describing the structure of ionic solids consist of two-body terms only,

$$V^{(2)} = \Sigma_{i>j}V_B^{(2)}(i,j) + \Sigma_{i>j}q_iq_j/r_{ij} \quad (47)$$

The short-range part has the Buckingham form,

$$V_B^{(2)}(i,j) = A_{ij}\exp(-r_{ij}/\rho_{ij}) + C_{ij}^{(6)} r_{ij}^{-6} \qquad (48)$$

They are known as rigid ion pair potentials.[4] For a good description of the TO_4 tetrahedra in zeolitic materials often a three-body term is added[50, 61] which includes the O—T—O angle bending force constant F_{ii}

$$V^{(3)} = V^{\text{angles}} = (1/2)\Sigma_i^{(T)} F_{ii}\left(\Theta_i - \Theta_i^0\right)^2 \qquad (49)$$

The sum runs over all six O—T—O angles of the TO_4 tetrahedron for a particular T site i. The reference angle Θ^0 usually is 109.47°. This term is typical for force fields rather than for ion-pair potentials, but it gives the TO_4 tetrahedra additional stiffness.

The most important many-body effects not included in the rigid ion-pair potential are polarization effects connected with the anion polarizability. They can be included[4] following the "shell-model" suggested by Dick and Overhauser.[62] The anions are represented by a pair of point charges, the positive core, and the negative and massless shell, which are connected by a harmonic spring,

$$V^{\text{core-shell}} = \Sigma_i k_i r_{c\text{-}s,i}^2 \qquad (50)$$

The spring constant k_i is related to the ion polarizability. A dipole is induced by the electric field originating from the point charges of all shells and cores of the crystal. Full formal charges (Si +4, Al +3, P +5, O −2) are used with the shell model potential. Not at all does this imply that bonding is fully ionic. It means only that using such charges an interatomic potential function can be defined that mimics the true PES. The advantage of shell model pair potentials is their good transferability that results in relatively few parameters. Their disadvantage is that they cannot easily describe molecules with directed bonds and, therefore, are not easily extended to zeolite–molecule interactions. Nevertheless, for the interaction of ammonia with the H-form of zeolites, $NH_3{\cdot}HZ$, and the ammonium form of zeolites, $NH_4^+Z^-$, a shell model potential has been derived[63] from *ab initio* data that can be used for combined QM-Pot calculations. Another example is the shell model potential description of H_2O molecules using parameters derived for O—H groups in titanosilicate models. This description is good enough to be used in a combined QM-Pot study of the hydration of TiO_4 sites in Ti-silicalite catalysts.[57]

The Reaction Force Field

Most interatomic potential functions approximate the potential energy surface around a single minimum that corresponds to a stable structure, but they are not globally valid for regions of the potential energy surface that connect one minimum with another through a transition region that corresponds to concerted bond rearrangements. We adopt Warshels empirical valence bond approach[64, 65] to join one interatomic potential function valid in the reactant valley to another one valid in the product valley. Neither of them is a realistic potential in the vicinity of the transition structure, but these potentials are considered as diagonal elements of a nonadiabatic electronic Hamiltonian that are coupled by a nondiagonal matrix element. For the latter, a suitable functional form is chosen that includes adjustable parameters obtained by a fit to *ab initio* results for the transition region of a model system. This *ab initio* parametrized EVB interatomic potential function describes the whole extended system, and is valid for all regions of the potential energy surface—from the reactant valley through the transition region to the product valley. When used in our combined QM-Pot scheme, the potential energy surface for a reaction in an extended system is further improved by an explicit quantum mechanical description of the reaction site. Hence, eq. (2) applies for the whole reaction surface, but the subscript "Pot" refers to the *ab initio*-parametrized EVB potential function.

The availability of such potentials is a great asset. A hierarchic strategy of finding transition structures in extended systems can be designed that first exploits the computationally less demanding parametrized EVB potential for getting starting information, and makes use of the combined QM-Pot method in a final refinement step only. A preliminary report of this strategy was given in a conference,[66] and the approach is described in detail in ref. 56. It provides a tool for calculating rate con-

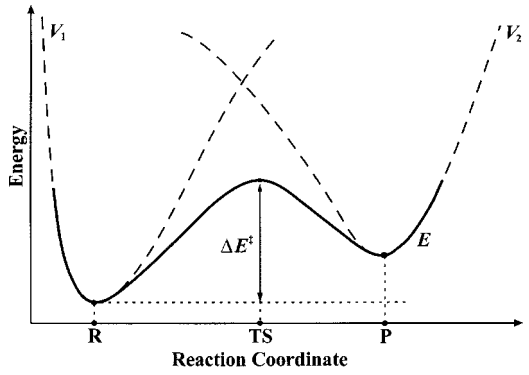

FIGURE 2. Interatomic potential functions for educts and products, coupled by EVB.

stants in extended systems with the same accuracy as can be achieved now for gas phase reactions for molecules of the size of the reaction site. An example for elementary steps in heterogeneous catalysis will be given below. To our knowledge, none of the QM-Pot (or QM/MM) schemes suggested so far has considered potential energy functions specifically designed for reactions including the transition region. The EVB coupling of interatomic potential functions by parametrized matrix elements has been suggested before by Chang and Miller[67] and recently also by Truhlar et al.[68]

In the simplest case, the EVB method proposed by Warshel considers two nonadiabatic states. The diagonal elements of the Hamiltonian are given by single minimum interatomic potential functions, V_1 and V_2, which describe the reactant and product states, respectively (Fig. 2). The nondiagonal element V_{12} couples these states, and the lowest root defines an adiabatic state that describes both the reactant and product valleys, as well as the transition region connecting them. The crucial part is the choice of the coupling element V_{12} that Chang and Miller calculate according to:[67]

$$\left[V_{12}(\mathbf{q})\right]^2 = A\exp\left(\mathbf{B}^T\Delta\mathbf{q} - \tfrac{1}{2}\Delta\mathbf{q}^T\mathbf{C}\Delta\mathbf{q}\right) \quad \text{with} \quad \Delta\mathbf{q} = \mathbf{q} - \mathbf{q}_0 \qquad (51)$$

$\mathbf{q}$ is the current structure and $\mathbf{q}_0$ is the reference structure in terms of internal coordinates. The scalar A, the vector $\mathbf{B}$, and the matrix $\mathbf{C}$ are chosen such that the energy, the structure, and the Hessian, respectively, calculated by a quantum mechanical method for the TS of the whole system, are reproduced. In line with the basic idea of the combined QM-Pot approach and differently from the original proposal we define V_{12} in terms of a small set of internal coordinates in which only atoms with the largest displacement along the reaction path are involved. This allows us to fit values of A, $\mathbf{B}$, $\mathbf{C}$, and $\mathbf{q}_0$ using quantum mechanical calculations on small cluster models for the TS, which makes the method applicable to extended systems. The fitted parameters are assumed to be transferable and used to describe the reaction in the extended system. Our modification of the method relies on the observation that the reaction coordinate usually involves only negligible motions of atoms sufficiently distant from the reaction site.

IMPLEMENTATION

The definition of the combined QM-Pot method by eq. (2) suggests a loose coupling of existing codes for evaluating the QM and interatomic potential contributions. This is one of the practical advantages of all hybrid QM/MM methods that rely on this equation, including, for example, Morokumas IMOMM and IMOMO methods. Our implementation of the method, the QMPOT code,[56] as its predecessors[8] including the commercial Solids_Embed[7] and QuanteMM software,[69] is basically an optimizer for minima and saddle points. External programs provide the energies and gradients for the QM and Pot parts, and communication is achieved through interface functions. Presently, interfaces are available for the QM codes TURBOMOLE,[70,71] GAUSSIAN94, GAUSSIAN98,[72] and DMOL[3] (ref. 73), and for the potential function codes DISCOVER,[74] OFF,[75] and GULP.[76] The latter is an efficient tool for lattice energy minimizations with the option to use shell-model ion-pair potentials.

The main features of QMPOT are: (a) fitting of EVB coupling element parameter, eq. (51), using *ab initio* data; (b) seam search (locating minimum energy points on the intersection line of two potential energy surfaces); (c) EVB and QM-Pot structure optimization to minima and saddle points; and (d) EVB and QM-Pot harmonic vibrational analysis.

The efficient trust region method[77–79] is implemented as optimization method that performs slightly better than the eigenvector following method of Baker,[80] at least for the set of molecules he examined.

For large chemical systems with many degrees of freedom, eqs. (6)–(8) suggest the following optimization protocol: (1) optimize to minima and saddle points using interatomic potential functions and EVB potentials, respectively, alone. Evaluate the Hessian matrix for the equilibrium structure found. (2) Optimize on the QM-Pot potential energy surface starting from the structure and Hessian obtained in cycle (1). Use QM-Pot gradients to update the Hessian. Moreover, in cycle (2) a significant reduction of the computational expense can be achieved by using microiterations in the following sense:[42,56,81] (a) first, positions of those atoms are optimized for which only the "Pot"-gradients have to be calculated [atoms of the outer part except those involved in the link atom definition, cf. eq. (8)], while the other atoms are kept at their positions. (b) Then, the combined QM-Pot gradients are calculated for the atoms of the active part, eqs. (7) and (11) and those atoms of the outer part that are involved in the definition of link atoms, eq. (12).

Cycles (a) and (b) are repeated until convergence is reached. Because the time needed to calculate the gradients for step (a) is negligible compared to the

time needed for step (b), the computational cost is determined by the number of degrees of freedom in the active part only. Moreover, step (a) can use techniques that do not require calculating a Hessian and, hence, avoid generation and diagonalization of very large matrices.

Convergence of the gradient norm within $0.0001 E_h a_0^{-1}$ can be achieved within 12 QM cycles for the minimum and within 20 QM cycles for the transition structure search of a system with 34 atoms in the quantum part and 289 atoms totally (Zeolite H-ZSM-5).[82] We stress that localizing the TS is achieved without explicit calculation of the QM Hessian for the inner part, which would be computationally very expensive.

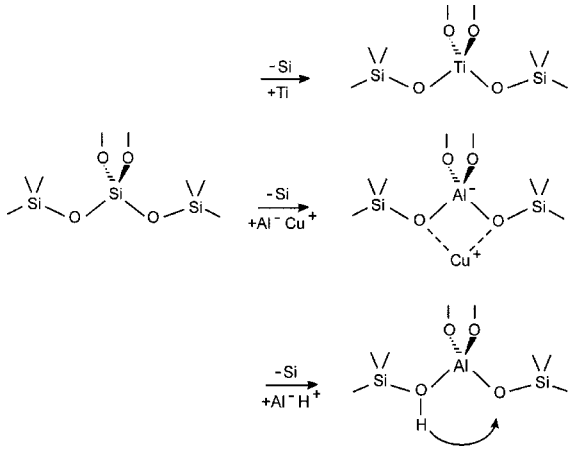

FIGURE 3. Active sites obtained by different substitutions into all-silica zeolite frameworks.

Applications—Structure and Reactivity of Zeolite Catalysts

INTRODUCTION INTO ZEOLITE CATALYSTS

Zeolites are microporous aluminosilicates of the composition

$$M_{x/n}\left[(AlO_2)_x(SiO_2)_y\right],$$

where M stands for metal cations. Today, the term zeolite is commonly used in a much broader sense. It includes all microporous materials that have three-dimensional networks made of corner-sharing TO_4 tetrahedra in which T is an electropositive component, typically Si, Al, or P. The large variety of materials[83] arises from (1) the many ways the tetrahedra can be connected to from networks with channels and cavities of different sizes; (2) the different type of cations present for charge compensation in extra-framework positions; (3) the different combination of cations in the tetrahedral framework positions (T = Si, Al, P, . . .).

One limiting case are "all silica" zeolites (SiO_2), which can also be considered microporous silica modifications. Due to the flexibility of the siloxane bond, Si—O—Si, rings of a varying number of SiO_4 tetrahedra (4–12) are easily formed while rings of three tetrahedra create some strain. The rings can be fused to form double rings or cages that are organized into networks with channels and cavities of molecular dimension. Figure 4 shows some structures that SiO_4 tetrahedra can build by sharing corners. Hypothetically, we obtain the regular zeolites from the all-silica zeolites if some of the Si^{4+} ions are replaced by Al^{3+} ions (Fig. 3). This formal process creates a negative charge on the framework that is compensated by extra-framework cations.

$$[SiO_2]_x + y\left(M^{n+}\right)_{1/n}Al^{3+} \rightarrow M_{y/n}\left[(AlO_2)_y(SiO_2)_{x-y}\right] + y SiO_2 \quad (52)$$

The Si/Al ratio, $(x-y)/y$, cannot be lower than 1. Neighboring pairs of AlO_4^- tetrahedra are forbidden by the Loewenstein rule. The extra-framework cations are easily exchanged.

Zeolites can aquire catalytic properties in a number of ways (Fig. 3). (1) Isomorphous substitution of Si^{4+} by other tetrahedrally coordinated cations, for example, the substitution of Ti into high-silica or all-silica zeolite frameworks creates highly selective oxidation catalysts. (2) Transition metal cations occupy extra-framework positions. Recently the use of Cu or Co exchanged zeolites in catalytic decomposition and reduction of NO_x was reported. (3) Zeolites become solid Brønsted acids if protons play the role of charge compensating cations. Protonated forms of zeolites are exceedingly important as industrial catalysts, for example, for hydrocarbon conversion in the petroleum industry. The most active catalysts include relatively few H/Al sites per Si, typically the Si/Al ratio, $(x-y)/y$, is 10 or larger. The proton forms of zeolites are obtained from the ammonium form by heating

$$(NH_4)_y\left[(AlO_2)_y(SiO_2)_{x-y}\right] \rightarrow \left[(H—AlO_2)_y(SiO_2)_{x-y}\right] + y NH_3 \quad (53)$$

Another class of microporous materials is obtained if—hypothetically—in a SiO_2 framework all pairs of SiO_4 tetrahedra are replaced by pairs of PO_4^+ and AlO_4^- tetrahedra. There is a strict P—Al alternation, which excludes all framework types having rings with an uneven number of TO_4

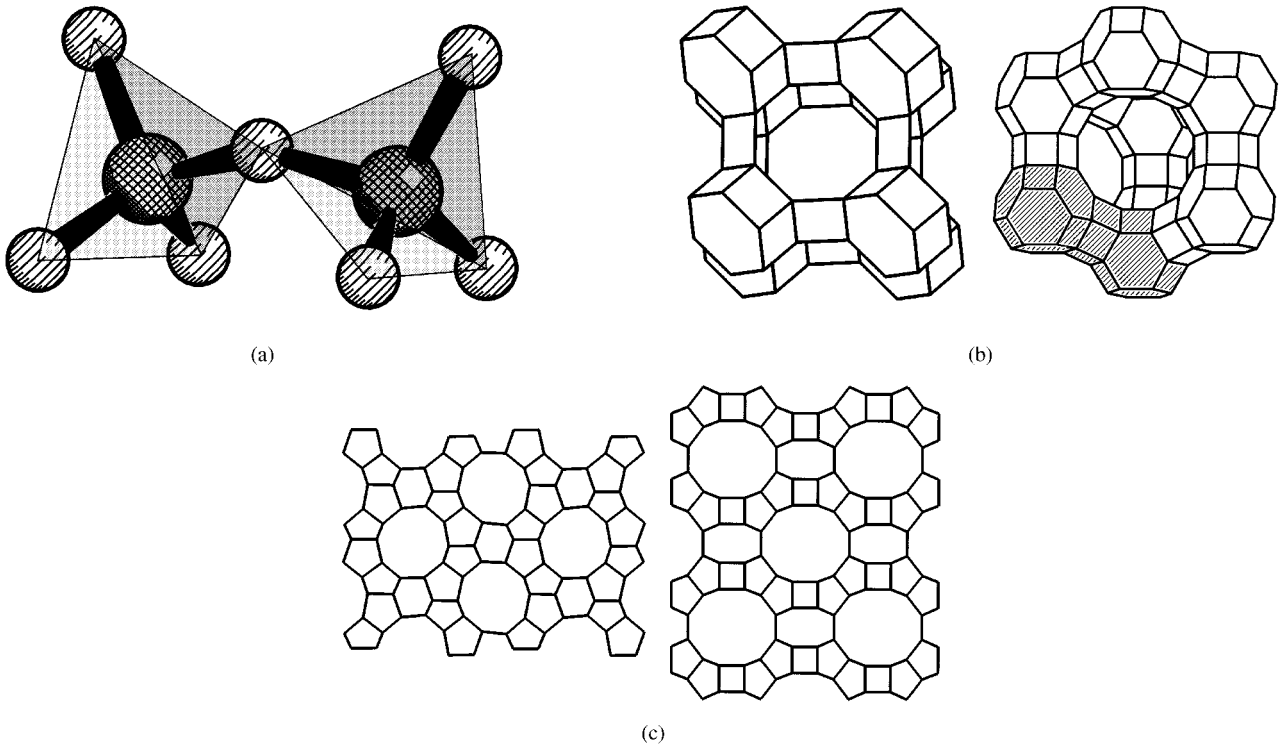

FIGURE 4. The basic building unit of zeolite frameworks, two corner-sharing TO_4 tetrahedra (a) and different zeolite framework structures, FAU and CHA (b), as well as MFI and MOR (c). Oxygen atoms are not shown for clarity.

tetrahedra, for example, five-membered rings. The neutral aluminium–phosphate frameworks (APO) become charged if P^{5+} is replaced by Si^{4+} (silicoaluminium–phosphates—SAPO) or if Al^{3+} is replaced by M^{2+} (M = Mg, Co, . . .—MeAPO). If the charge is compensated by protons, we have again Brønsted sites and materials that are solid acids.

Typical of the crystal structure of zeolites is the large number of atoms they have in the unit cell. Table II summarizes some information about zeolites of interest in the present article. While some frameworks have high symmetry and only few crystallographically distinct sites (CHA, FAU), others have low symmetry and a large number of crystallographically distinct sites. One of the most interesting frameworks is MFI. In its orthorhombic high-temperature modification there are 12 distinct T sites, while the monoclinic low-temperature modification has 24 different T sites. As Al (or Ti) can be substituted in any of these sites and the charge compensating cations can occupy different extra-framework sites, there is a large variety of possible sites. Only in exceptional cases the location of the active site is exactly known, for example, in FAU there is only one crystallographically distinct T site (in which Al can sit), but there are four possible oxygen sites. Spectroscopy in combination with selective adsorption revealed that protons occupy preferentially the O1 and O3 sites, and that protons at these sites give rise to the so-called high frequency and low-frequency IR bands. But even in this framework, the number of possibilities increases when the Al content increases beyond one atom per unit cell.

The key questions that could not be answered so far by experiments are: are there preferred sites within the crystal lattice for the catalytically active site, and does the location of the active site affect its catalytic activity? Answering these questions is a challenge for computational quantum chemistry. It is clear from the beginning that cluster calculations are not suitable. They cannot describe the differences in the activity of a given active site due to different positions in the lattice, which requires a method that can model both the different structure constraints and the different crystal potentials at different positions. *Ab initio* calculations applying periodic boundary conditions just now become applicable to crystalline materials with unit cells as large as MFI has, but they cannot be routinely used for the large number of exploratory calculations. The combined QM-Pot method is ideally suited for such projects. *Ab initio*-parametrized

TABLE II.
Some Zeolite Structures.

Common Name	Code[a]	Rings[b]	Space Group	Size of Conventional u.c. (Å)	Atoms per u.c.[c]	Atoms per p.c.[d]	Distinct Sites T	Distinct Sites O
Faujasite (Y)	FAU	12; 6	Fd3m	24.6 × 24.6 × 24.6	576	144	1	4
ZSM-5, Silicalite	MFI	10	$P2_1/n.1.1$	20.4 × 20.2 × 13.6	288	288	24	48
			Pnma				12	26
Mordenite	MOR	12; 8	Cmcm	18.3 × 20.5 × 7.6	144	72	4	10
Chabazite	CHA	8	$R\bar{3}m$	13.7 × 13.7 × 14.8	108	36	1	4

Data neglect extraframework cations and do not distinguish between Si and Al atoms.
[a] Ref. 83.
[b] No. of T—O bonds in the $(T—O)_n$ rings defining the micropores.
[c] Unit cell.
[d] Primitive cell.

ion-pair shell-model potentials are available that describe the periodic structure of zeolite frameworks very accurately. When a QM cluster for the active site is embedded at different crystallographic positions in the lattice described by these potential functions, a very good description of the differences is achieved. Figure 5 shows different sites of Cu^+ ions in CuZSM-5 (MFI framework) that have been determined by the combined QM-Pot method.[54]

Hence, the QM-Pot method appears to be a unique tool that can be used to study the effect of the bulk structure of the reactivity of active sites.

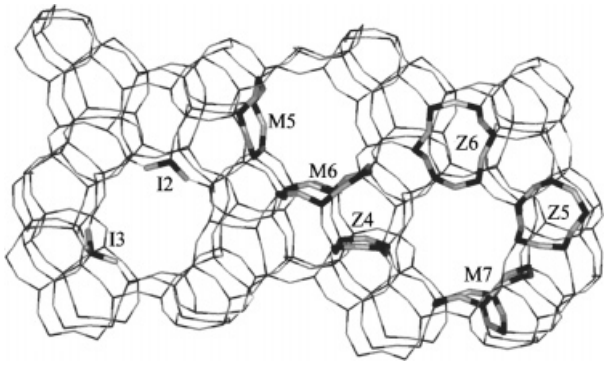

FIGURE 5. Different Cu^+ sites in the Cu-ZSM-5 catalyst. The labels refer to the number of framework oxygen atoms defining the site and to their location in the channel system (M and Z—main and zigzag channels, I—channel intersection). View at the (010) layer, the 10-membered T-O rings form the walls of the main channel. The sites are found by combined QM-Pot calculations. Reproduced by permission of The Royal Society of Chemistry.

TRANSITION METAL CATIONS AS ACTIVE SITES IN ZEOLITE CATALYSTS (CuZSM-5)

The observation that CuZSM-5 is a particularly active catalyst in the selective NO_x decomposition triggered a multitude of experimental and computational studies. There were indications that different types of sites exist, but the nature of these sites and their location in the framework was not clear. The combined QM-Pot study of the siting and coordination of Cu^+ in ZSM-5 adopted a two-stage strategy. First, the DFT-parametrized ion-pair shell-model potential function for aluminosilicates[37] was used to do lattice energy minimizations for the MFI framework with just one Al in a T-site (no charge balancing cation). The difference between the most (Al in T1 position) and the least stable structures (Al in T6 position) was 36 kJ/mol only. For each of the Al sites considered at least 10 lattice energy minimizations with different starting Cu^+ positions were made, again using the potential alone. Second, for 12 of the 34 local minima found, refinement of the results was made by combined QM-Pot calculations. Quantum clusters of different size were used, depending on the number of direct Cu^+—O(framework) contacts. Although the absolute values of the Cu^+ binding energies increased by 40–70 kJ/mol, the Cu—O distances were very similar and the coordination numbers changed only in a few cases.

The sites obtained were classified according to the number of framework O atoms having a direct coordination (oxygen atoms within 2.5 Å of Cu^+). According to this definition, there are two types of sites. In type II sites Cu^+ is coordinated to two O atoms of the AlO_4 tetrahedron. Type II sites occur

at the channel intersection only, and are denoted I2. Type I sites have one or two additional coordinations to other framework oxygen atoms within a five- or six-membered $(TO)_n$ ring. We label them according to the size of the ring (five or six, seven denotes a six-membered ring with a bridging tetrahedron) and the type of the channel (M—main or straight channel, Z—sinusoidal or zig-zag channel), at the wall of which the $(TO)_n$ ring is located. For example, when Al is in the T1 site, Cu^+ can occupy an I2 site or an M7 site. The predicted difference in stability is 6 kJ/mol only (QM-Pot results). These findings are in agreement with EXAFS studies, for example, of Lamberti et al.,[84] who report a coordination number of 2.5 ± 0.3. While EXAFS provides an average picture, the *ab initio* simulations yield individual pictures of two types of sites involved. The existence of two different types of sites also emerges from photoluminescence studies.[84] While the $3d^{10}(^1S_0) \rightarrow 3d^9 4s^1(^1D_2)$ excitation spectra show two well-separated bands, the band splitting almost disappears in the emission spectra. The calculated[85] transition energies show the same behavior. Note that for technical reasons the calculations have been performed for the $3d^9 4s^1(^3D_2)$ triplet state, while in experiments excitation is into the corresponding singlet state, and only the emission is from the triplet state. Relative energies are not expected to be affected, however. The calculations[85] do not only reproduce the trends in the excitation energies, they also provide an explanation. Emission occurs from relaxed excited state structures. Hence, structure optimizations have been made by the combined QM-Pot method for the excited state. While type II sites virtually do not change, type I sites give up their additional coordination and retain only the twofold coordination to the AlO_4 tetrahedron. The reason is that on excitation an electron occupies the 4s orbital, which is much larger than the 3d orbital, and the Cu^+ ion moves away from the channel walls. Hence, the difference between type I and type II sites is virtually lifted in the excited state and the emission energies become very similar. Figure 6 shows the coordination change on excitation for the M7 site with Al in the T1 position. Note the large changes of the T—O—T bond angles in the $(TO)_6$ ring. This stresses that neither a free space cluster calculation nor a frozen lattice cluster calculation could satisfactorily describe such phenomena.

Of course, the most interesting question is if the reactivities of the two types of sites are different. Do they play a different role in the catalytic process? As a first step in this direction, adsorption of NO at Cu^+ sites has been studied by the combined QM-Pot method.[86] A similar effect of NO adsorption on the structure is observed as on excitation. While the structure of the type II sites (I2) is not affected, in the type I sites (Z6, M7) Cu^+ gives up the additional coordinations to non-AlO_4 framework oxygen atoms in favor of optimum binding of NO. This reduces the total binding energy as seen in Table III. As a result, the binding of NO to Cu^+ sites of type I in zeolites is smaller than the binding to gas phase Cu^+ ions, only type II sites (I2) in CuZSM-5 bind NO stronger than gas phase ions. This is also true for the binding of NO_2 onto type II sites.[87] A rationale of this "activation" of Cu^+ ions in zeolite catalysts is given in ref. 87. It remains to be seen how much the barrier for all steps of the catalytic cycle are affected. It is completely clear that free space cluster models as exclusively used in previous studies of possible catalytic cycles[88–90] fail to reveal differences between different sites. Table III

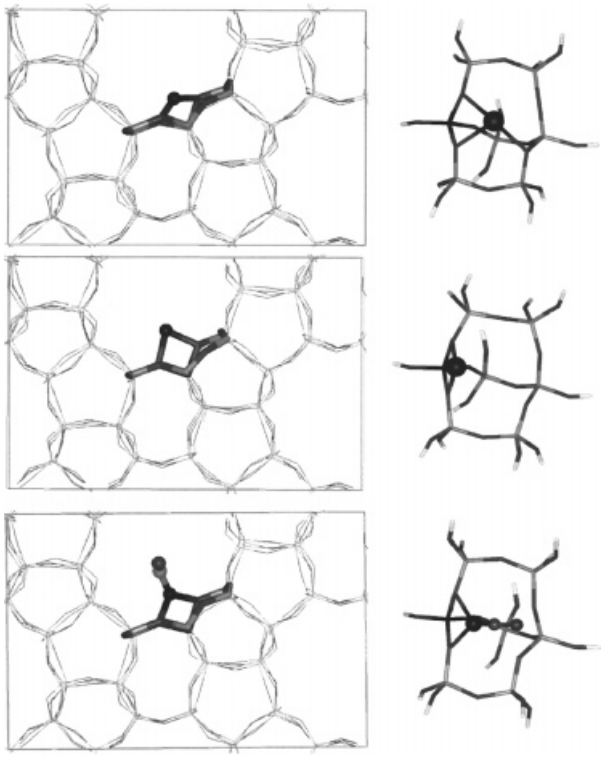

FIGURE 6. Type I Cu^+ site in CuZSM-5 (M7 with Al in T1 position). The left panels show the side view on the QM cluster embedded in the periodic zeolite structure described by an ion-pair shell-model potential. The right-hand side provides top views on the QM clusters without showing the embedding lattice. Top: electronic ground state; middle: electronic excited state from which emission occurs; bottom: structure after adsorption of NO.

TABLE III.
Comparison of Embedded QM-Pot[a] and Free Space Cluster Results for NO Adsorption on Different Cu^+ Sites in Cu-ZSM-5.

Site[b]		CN all O/O_{Al}	r(Cu—N)	ΔE
Type I	Z6/T4	$4 \rightarrow 2/2$	179	110
	M7/T1	$3 \rightarrow 2/2$	181	117
Type II	I2/T2	$2 \rightarrow 2/2$	181	140
$\{Cu^+3T^-\}_Z$[c]			181	139
$\{Cu^+Al(OH)_4^-\}_Z$			181	142
$\{Cu^+(H_2O)_2\}_Z$			185	128
$Cu^+(H_2O)_2$			186	46
Cu^+				129

Coordination number, CN, bond distance, r(Cu—N) in pm, and dissociation energy, ΔE in kJ/mol. Results from ref. 86.
[a] B3LYP/T(O)DZP.
[b] $\{\ldots\}_Z$ means at the structure of I2/T2.
[c] $3T^- = [(HO)_3SiOAl(OH)_2OSi(OH)_3]^-$.

illustrates that clusters as small as $Cu^+Al(OH)_4^-$ are able to reproduce the NO binding itself, but only if the proper structure of the complex is known from combined QM-Pot calculations. Use of two water ligands as a free-space cluster model fails badly. If the water molecules are forced to the orientation that corresponds to the O site configuration of the zeolite framework, the results are in the right range, but still do not reproduce the enhanced binding compared to naked Cu^+ ions in the gas phase.

ACIDIC ZEOLITE CATALYSTS

Zeolite acidity can be characterized by different model reactions.

(1) Deprotonation

$$ZO—H \rightarrow ZO^- + H^+ \quad (54)$$

This hypothetical process defines gas phase acidities.

(2) Chemisorption of NH_3

$$ZO—H + NH_3 \rightarrow ZO^-NH_4^+ \quad (55)$$

This process can be studied by microcalorimetry, and the reverse process is observed in temperature-programmed desorption experiments.

(3) Proton jumps between two oxygen atoms of the same AlO_4 tetrahedron (indicated by the arrow in Fig. 3).

$$Z(O_2)O_1—H \rightarrow Z(O_1)O_2—H \quad (56)$$

By definition, the reaction energy for proton jumps is obtained from the deprotonation energies of the two sites involved by subtraction. The barrier and the corresponding jump rate characterize the proton mobility of the active site.

In this chapter applications of the QM-Pot method will be reviewed for all three types of reactions. Whenever possible, comparison will be made with the full periodic limit obtained by codes that apply periodic boundary conditions to the *ab initio* method, and the convergence of the QM-Pot results with increasing size of the quantum cluster will be studied. In this respect, the decomposition of the reaction energies into the direct quantum mechanical contribution, and a long-range correction, eq. (39), will be very illuminating. Generally, we expect the long-range correction to decrease with increasing size of the QM cluster, but it turns out that the size of the long-range correction also depends on the shape of the cluster and its specific location in the crystal lattice. QM-Pot reaction energy calculations for deprotonation and NH_3 chemisorption can be completed with single minimum potential energy surfaces. Note, however, that the interatomic potential functions used for the reactants and the products are different due to different atom types. In refs. 46, 63, and 91 it is argued that this is not a problem as long as the quantum part is large enough to include all short-range contributions. When proton jump rates and energy barriers are the target instead of reaction energies, the potential energy surfaces of reactants and products have to be coupled by EVB as described in the Reaction Force Field section.

Energies of Deprotonation and NH_3 Chemisorption

Gas phase acidity is defined as enthalpy of deprotonation, and relative values for gas phase molecules are experimentally accessible from proton transfer equilibrium data. For acidic sites at surfaces such data are only provided by calculations. Experimentally, inferences can only be made from spectroscopic data. We first look at the convergence of QM-Pot results with respect to the size of the embeded quantum clusters. Table IV shows for H-faujasite the expected decrease of the long-range correction with increasing size of the cluster (from -119 to -52 kJ/mol). This does not mean that the long-range effects disappear. Rather, an increasing share of them is included in the QM result for the cluster. The combined QM-Pot result is remarkably stable; for all cluster sizes studied it varies between 1250 and 1253 kJ/mol only. The results for MFI,

TABLE IV.
Dependence of Deprotonation Energies (kJ/mol) on the Size of the QM Cluster (HF/T(O)DZP).

Zeolite	Cluster[a]	ΔE_{QM}	ΔE_{LR}	$\Delta E_{QM\text{-}Pot}$
FAU	2T	1369	−119	1250
	3T	1354	−102	1252
	4R-1Al	1348	−98	1250
	shell-3//3T[b]	1331	−78	1253
	shell-5//3T[c]	1303	−52	1251
MFI	2T	1363	−77	1286
	3T	1357	−70	1287
	5R	1344	−62	1282
	6T	1350	−69	1281
	8T//6T	1352	−71	1281
	10T//6T	1356	−70	1286
	14T//6T	1358	−75	1283
	28T//6T	1326	−44	1282

Data taken from refs. 46, 63, 91, and 92.
[a] See the original articles for the shape of the cluster models.
[b] Shell-3 means a model consisting of three complete coordination shells around the central Al atom, $Al^{-}[OSi(OH)_3]_4$. It is also known as the pentameric cluster model.
[c] Shell-5 models include five complete coordination shells around the central Al atom.

also included in Table IV, do not show as good a convergence. When embedding a quantum cluster of 14 tetrahedra (14T) the long-range correction is almost as large as when embedding a very small cluster of two tetrahedra only (2T). Only when the cluster includes as many as 28 tetrahedra the long-range correction is significantly reduced (from −75 to −44 kJ/mol). Nevertheless, also in this case the total QM-Pot results stay within a narrow range of 1287–1281 kJ/mol for all sizes of embedded clusters. That even for the largest clusters the long-range corrections are as large as 44 kJ/mol underlines that these effects must not be neglected, and that calculations of small gas phase models are of little predictive value. It has been noted[63] that relatively small cluster models sometimes yield results that are apparently in good agreement with QM-Pot results for embedded clusters or with periodic *ab initio* results. The explanation is that artificial structure relaxation effects due to missing lattice constraints may partially compensate neglected crystal potential contributions.

The embedded cluster QM-Pot results for Brønsted sites in different frameworks[46, 91, 92] (Table V) permit one to establish an acidity scale. One should keep in mind, however, that deprotonation energy is one among different parameters that may be used to characterize solid-state acidity. When comparison is made between results obtained by different methods, for example, HF or a particular density functional, the different systematic errors of the different approaches must be eliminated. This is done by defining a correction constant for each of the methods.[93] These constants are obtained by calibration calculations of the deprotonation energies for silanol and methanol, related molecules for which very accurate values are known. Table V shows such

TABLE V.
Energies of Deprotonation (kJ/mol) Calculated by Different Methods for Brønsted Sites of Different Zeolite Catalysts.[a]

Zeolite		QM-Pot HF corr.[b]	QM-Pot B3LYP[c]	QM-Pot BLYP corr.[d]	Plane Wave BLYP corr.[e]
HSAPO-34	CHA		1261	1280	1276
H-ZSM-5	MFI	1235			
H-MOR	MOR	1230			
H-SSZ-13	CHA	1225	1231	1233	1235
H-Y[f]	FAU	1220[f]	1224[f]		
H-Sil	FAU	1206	1198		

[a] To eliminate the effect of different systematic errors in the different approaches, a constant is added for each of the methods. These constants are obtained by calibration calculations of the energies of methanol and silanol, related molecules for which very accurate values are known.
[b] Corrected by −46 kJ/mol.[93] Data from refs. 46 and 91.
[c] No correction is necessary. The systematic error appears to be zero. Data from refs. 37 and 53.
[d] Corrected by 8 kJ/mol. Data from ref. 53.
[e] Corrected by 38 kJ/mol. Data from ref. 53.
[f] A four-ring model describing a next nearest neighbor pair of Al was embedded in a periodic structure of the Si/Al ratio of 3. Data from ref. 92.

data. After correction, HF and B3LYP results agree within 4–8 kJ/mol. This approach can also be used to compare combined QM-Pot results with periodic DFT calculations that use plane wave basis sets and describe inner shell electrons by pseudopotentials. For two chabazite catalysts of different composition (the aluminosilicate material H-SSZ-13 and the silico-aluminium–phosphate material H-SAPO-34) we find excellent agreement (within 4 kJ/mol) between the combined QM-Pot result and the full *ab initio* calculations that apply periodic boundary conditions.[53] This confirms that the combined QM-Pot method takes the long-range effects properly into account.

Comparison with free cluster models is meaningful only if the models are very large. There are two such studies in the literature. One completely optimizes a 48 tetrahedra model of H-FAU (two sodalite cages bridged by a double six-membered ring, cf. Fig. 4) and arrives at a corrected deprotonation energy of 1198 kJ/mol in excellent agreement with the 1206 kJ/mol in Table V.[94] The other uses different 38 tetrahedra models to extrapolate the result for a 46 tetrahedra model of ZSM-5.[29, 95] After additional corrections it arrives at a result of 1267 kJ/mol, somewhat larger than the corrected QM-Pot value of 1229 kJ/mol. (The result of 1235 kJ/mol in Table V holds for a different crystallographic position.[91]) The larger deprotonation energy indicates that not all long-range stabilization effects or not all structure relaxation effects may be included in the calculations of refs. 29 and 95. Only the inner 10 atoms of the cluster were optimized.

Before comparison can be made with deprotonation enthalpies derived from experiments (frequently given as proton affinities of the conjugated anion), nuclear motion corrections have to be added which are estimated to about $-30 \ldots -35$ kJ/mol.[29, 46]

While from the experimental point of view there is no doubt that NH_3 is protonated at zeolitic Brønsted sites, to correctly reproduce the sign for the reaction energy of the proton transfer process,

$$\mathrm{ZO{-}H{\cdot}NH_3} \rightarrow \mathrm{ZO^-NH_4^+} \qquad (57)$$

by calculations proved difficult. An analysis[96] revealed that this was mainly due to too small basis sets.

Table VI shows results for a typical case, adsorption of NH_3 in zeolite faujasite. The combined QM-Pot method correctly predicts that the $NH_4^+Z^-$ form is more stable than the $NH_3{\cdot}HZ$ form by about 35 kJ/mol. The adsorption energy is 106 kJ/mol. There are significant long-range corrections due to the embedding ion-pair shell-model potential. Another combined QM-Potential function approach that differs in many details from our QM-Pot method yields very similar results,[97] while a more recent study that uses another version of the com-

TABLE VI.
Chemisorption of NH_3 on Bridging Hydroxyls of H-Faujasite: NH_3 + H-FAU → $NH_4^+FAU^-$.

	Free Space Cluster Models		Combined QM–Interatomic Potential Function Methods					
Model	Basis Set	ΔE	Framework	Method	Basis Set	ΔE	ΔE_{LR}	ΔE_{QM}
shell-2	T(O)DZP	−56[d]	FAU	QM-class[a]	6-31G*	−86		
shell-1.5	6-31G**	−72	FAU	QM-class[b]	6-31G**	−110	(−38)[c]	(−72)[c]
shell-1.5	T(O)DZP	−67[d]	FAU					
3T	T(O)DZP	−92[e]	FAU	QM-Pot[e]	T(O)DZP	−106	−48	−58
shell-3//3T			FAU	QM-Pot[e]	T(O)DZP	−107	−44	−63
shell-5//3T			FAU	QM-Pot[e]	T(O)DZP	−106	−25	−81
8T (ring)	T(O)DZP	−56	CHA	QM-Pot[e,f]	T(O)DZP	−109	−45	−64
			CHA	periodic HF[f]	T(O)DZP	−100		

HF calculations on cluster and embedded cluster models (QM-Pot). Energies in kJ/mol.
[a] Combined QM-classical calculation, ref. 98, optimization limited to a shell-5 cluster.
[b] Combined QM-classical calculation, ref. 97, optimization limited to the AlO_4-unit of the QM cluster.
[c] Decomposition into QM part and contribution from the embedding potential is not available. Estimates have been obtained from the result for the nonembedded cluster with the AlO_4 part optimized.
[d] Ref. 96.
[e] Combined QM-Pot method, full optimization of the periodic structure.
[f] Ref. 99.

TABLE VII.
Proton Jump Reaction Energies and Reaction Barriers for H-Chabazite (kJ/mol).

	ΔE			$\Delta E^{\ddagger}$			$\Delta E^{\ddagger}_{LR}$	
Jump Path	Full QM	8T	3T/4T	Full QM	8T	3T/4T	8T	3T/4T
O3—O4	3.3	1.7	−5.6	69	65	71	9.2	17.4
O1—O2	11.5	11.2	21.7	72	66	76	−12.2	24.5
O1—O3	7.2	3.6	8.5	90	90	96	13.6	42.1
O3—O2	3.8	3.5	7.9	92	87	97	11.0	34.0
O2—O4	3.2	0.2	−9.6	97	99	97	55.5	41.6
O1—O4	13.4	12.4	5.8	105	102	105	7.2	26.4
(max error)		(3.6)	(12.8)		(6)	(6)		

Combined QM-Pot results compared to fully periodic quantum calculations (B3LYP/T(O)DZP) (ref. 56).

bined method and a basis set without polarization functions on the H atoms reports a significantly smaller value of 86 kJ/mol.[98] Although a periodic structure optimization was not possible, for the zeolite chabazite a periodic HF calculation was made using the CRYSTAL code.[99] By definition, the long-range *correction* is zero in the periodic calculation, which does not mean, of course, that the long-range electrostatic interactions are zero. The adsorption energy deviates from that of the embedded cluster QM-Pot calculation with the same basis set by 9 kJ/mol only (Table VI). The periodic HF calculation was made as a single point calculation using the structure found by the combined QM-Pot approach. Comparison with observed data is also favorable. After adding estimates for the electron correlation (from cluster calculations) and for nuclear motion effects, a value is predicted for the heat of adsorption that is at the lower edge of observed data.[91]

Comparison of the Mobility of Brønsted Protons in Different Zeolites

The rates of proton jumps between the four oxygen positions of the AlO_4 tetrahedron (cf. Fig. 3, bottom) determine the on-site proton mobility in zeolites. Theoretical predictions of these rates require localization of all four minima and all six transition structures for a given crystallographic site. The differences between different zeolite frameworks and different crystallographic sites can only be revealed if a method is used that takes the periodic zeolite structure into account. Our combined QM-Pot approach is such a method. From the energies of the stationary points reaction energies and energy barriers are calculated. We first discuss the error of the QM-Pot results for reaction energies and energy barriers. For the small unit cell zeolite chabazite comparison with full periodic quantum mechanical calculations is possible (Table VII). Cluster models of two sizes are embedded (Fig. 7). The smaller models consist of three or four TO_4 tetrahedra, depending on the jump path studied. The larger model is the same for all paths. It consists of eight tetrahedra, and is formed by three annealed $(TO)_4$ rings. For the reaction energy the maximum error is re-

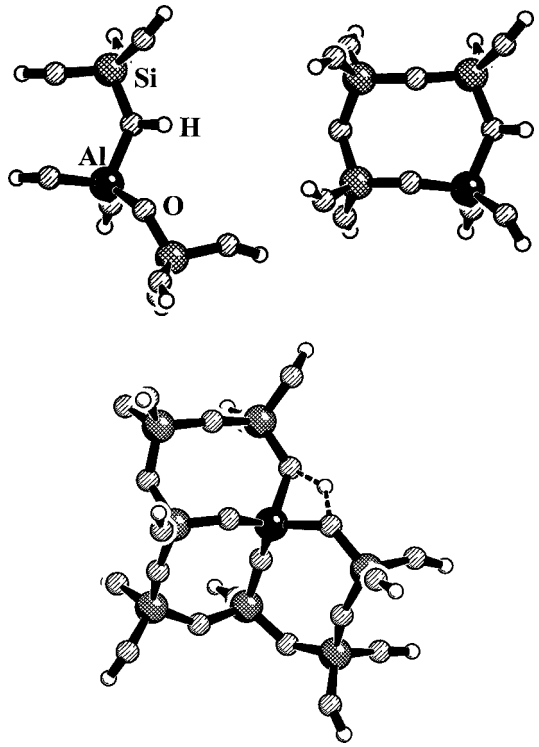

FIGURE 7. Embedded cluster models (the embedding lattice is not shown) used for QM-Pot calculations on proton jump reactions in H-chabazite. Top: 3T/4T models; bottom: 8T model.

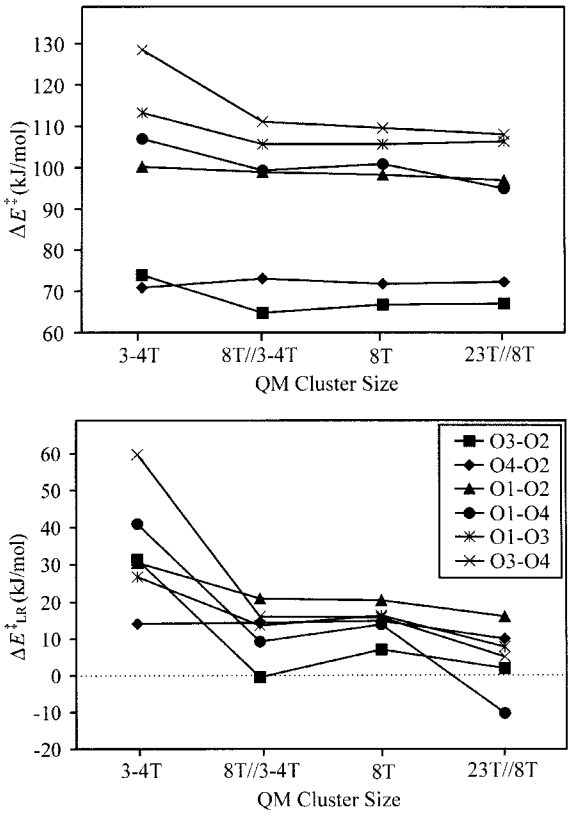

FIGURE 8. Dependence of the QM-Pot proton jump barrier (top) on the size of the embedded cluster for different jump paths in H-faujasite. XT//YT means single-point energy obtained for embedding an XT cluster at a structure obtained by QM-Pot optimizations when embedding a YT cluster. The lower part of the figure shows the size for the long-range *correction*, which should converges towards zero when approaching the periodic QM limit.

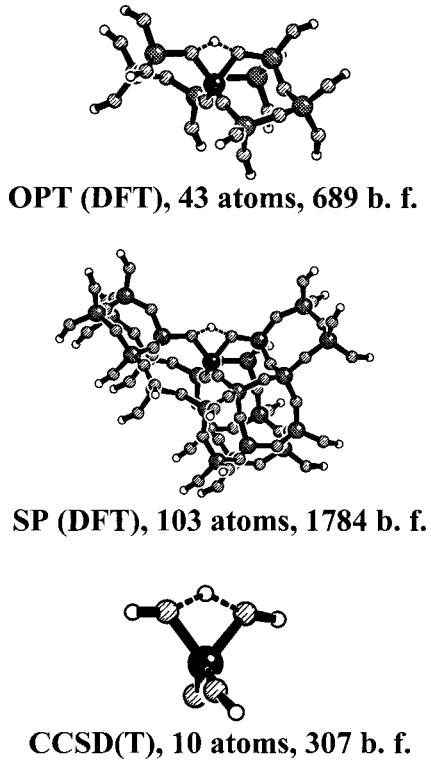

FIGURE 9. Different clusters used for quantum mechanical calculations of proton jump barriers. Top: cluster model used in the combined QM-Pot transition structure optimization. Middle: cluster model used for combined QM-Pot single point calculation. Bottom: cluster model used in CCSD(T) calculations for estimating the accuracy of the DFT method used (B3LYP/T(O)DZP).

duced from 13 to 4 kJ/mol when passing from the small to the larger quantum part. For the reaction barrier the maximum error is 6 kJ/mol independent off the cluster size. The long-range correction to the barrier, ($\Delta E^{\ddagger}_{LR}$), becomes smaller when the cluster size increases (with one exception), but it shows large variations even for the larger cluster. It is not only the cluster size that determines the long-range correction, it is also the cluster shape. Use of cluster models of the same size without embedding will produce large errors on the relative barrier heights.

This is also true for H-faujasite. Figure 8 compares QM-Pot results obtained with embedded clusters of different size (see Fig. 9). Even for the largest clusters, compraising 23 tetrahedra, the long-range corrections vary over 25 kJ/mol, while for the smaller 8T models they vary over about 15 kJ/mol only. This points to the important effect of the cluster shape on the size of the long-range correction. Due to the combined QM-Pot method, the total barrier heights are stable within a few kJ/mol.

Because of the importance of the long-range corrections we have adopted the following computational strategy: (1) Optimization of minima and transition structures by the QM-Pot approach using 8T embedded clusters. (2) Energies are refined by single-point QM-Pot calculations for 23 T embedded clusters at the structures obtained in step (1). (3) To correct for the approximations connected with the B3LYP density functional and the modest basis set adopted, we made CCSD(T)/cc-pVTZ calculations on very small 1T cluster models and compare the results with B3LYP/T(O)DZP results. The 1T models consist of a single AlO_4 tetrahedron (Fig. 9), and are cut out of the structure obtained in step (1). Details are given in the original article.[82] The corrections on the barriers for different paths vary

between 4 and 15 kJ/mol. The barriers themselves vary between 67 and 108 kJ/mol.

Vibrational analysis is made to characterize the stationary points. It also yields the vibrational partition functions from which the rate can be calculated using the classical transition state theory. This way, proton rates have been calculated for Brønsted sites of different protonated zeolites, chabazite (CHA), faujasite (FAU), and ZSM-5 (MFI). The predicted jump rates show large variations, from 10^{-6} to 10^{5} s^{-1} at room temperature, and vary between different jump paths for a given site and between Brønsted sites in different frameworks. The QM-Pot results were also used to estimate the temperature below which tunneling becomes important and above which tunneling becomes negligible. For all jump paths considered, these crossover temperatures are lower or equal room temperature. The highest temperature was 320 K. Hence, tunneling is not an important factor above room temperature. This study is a complete *ab initio* prediction of reaction rates for an elementary surface process of a complex heterogeneous catalysts and of how these rates differ between different catalysts.[82] It could only be achieved because of the power of combined QM-Pot methods.

Other Hybrid QM/MM Studies

As mentioned before, this article does not aim at a general review. Applications of the method to homogeneous catalysis have been reviewed by Woo et al., who use the combined QM/MM approach in the *ab initio* molecular dynamics mode.[18] Froese and Morokuma describe the use of their IMOMM method in a study of substituent effects in nickel diimine catalysts.[12] Our combined QM-Pot method has also been used to examine the rac-meso configurational stability and rotational transition in zirconocene-based Ziegler-Natta catalysts.[100]

In this section we will briefly mention some applications of hybrid QM/MM methods for surface problems. The IMOMM method[42] without any customization was tested in a study of Cu atom deposition on SiO_2 surface defects (E' surface center, $Si^{\bullet}$, and NBO center, $SiO^{\bullet}$).[101] Small clusters representing one or two Si sites were embedded in medium-sized clusters. Because the terminating hydrogen atoms of the MM cluster were fixed, the results suffered from some strain in the MM part.

SIMOMM,[45] a special brand of the IMOMM method, has been designed for surface problems, and methods aspects have been already discussed in the LINK ATOM section. It does not apply periodic boundary condition and uses large, but finite cluster models for the MM part, for example, a $Si_{38}H_{36}$ cluster is used to model the silicon surface. The method was used to examine the cycloaddition reactions of 1,3-cyclohexadiene on the silicon(001) surface.[102] Weiner's combined QM-Pot method,[44] which has been presented in the LINK ATOM section, was extensively used in studies of reactions on silicon and diamond surfaces.[103–107]

The alkene chemisorption in chabazite has been studied by a combined QM-classical method.[108] The quantum cluster is terminated by hydrogen link atoms, but no attempt is made to correct the combined QM-Pot potential or its derivatives for the contributions from these link atoms. Hence, the scheme is similar to those defined by eqs. (16) and (27). The zeolite framework is described by our *ab initio*-parametrized CFF force field[52] and the zeolite–hydrocarbon interactions by the potential functions derived by Nicholas et al.[109]

Shluger and Gale[10] used a combined QM-Pot method for studying defects in ionic crystals. It is based on a subtraction scheme that differs from eq. (2) in two respects. (1) There are no link atoms, but point charges are added to the quantum cluster. (2) Part of the E(I-O) interaction term, the long-range (LR) part, is calculated quantum mechanically, while the remaining, short-range (SR) contributions are calculated by the potential function,

$$E_{\text{QM-Pot}}(S) = E_{\text{QM}}(\text{I}) + E_{\text{Pot}}(\text{O}) + E_{\text{QM}}(\text{I-O})_{\text{LR}} + E_{\text{Pot}}(\text{I-O})_{\text{SR}}. \quad (58)$$

The quantum calculations are made on the cluster with the Hamiltonian including the additional point charges of the outer part. If we formally replace the link atoms, L, in our scheme by the point charges, P, of the environment, $C = \text{I} + P$, we can write

$$E_{\text{QM}}(C) = E_{\text{QM}}(\text{I}) + E_{\text{QM}}(\text{I-O})_{\text{LR}} \quad (59)$$

The potential function is applied to both the whole system S and the I part. In addition, the Coulomb part of the potential function interaction between the ions of the inner part and the environment, $E_{\text{Pot}}(\text{I-O})_{\text{LR}}$, is calculated. Similar to eq. (59) we may define

$$E_{\text{Pot}}(C) = E_{\text{Pot}}(\text{I}) + E_{\text{Pot}}(\text{I-O})_{\text{LR}} \quad (60)$$

Since

$$E_{\text{Pot}}(S) - E_{\text{Pot}}(\text{I}) - E_{\text{Pot}}(\text{I-O})_{\text{LR}} = E_{\text{Pot}}(\text{O}) + E_{\text{Pot}}(\text{I-O})_{\text{SR}} \quad (61)$$

and see that eq. (58) is identical with eq. (2)

$$E_{\text{QM-Pot}}(S) = E_{\text{QM}}(C) + E_{\text{Pot}}(S) - E_{\text{Pot}}(C) \qquad (62)$$

The method has also been used to study the processes at ionic surfaces induced by atomic-force microscope tips.[110]

Acknowledgments

This work has benefited from the Catalysis and Sorption Project of Molecular Simulations Inc., San Diego, CA. We are grateful to Dana Nachtigallová and Petr Nachtigall (Prague) for the permission to use unpublished data, and to Max Holthausen for comments on the manuscript.

References

1. Burkert, U.; Allinger, N. L. Molecular Mechanics; American Chemical Society: Washington, DC, 1982.
2. Maple, J. R. In Encyclopedia of Computational Chemistry; von Ragué Schleyer, P.; Allinger, N. L.; Kollman, P. A.; Clark, T.; Schaefer, H. F., III; Gasteiger, J.; Schreiner, P. R., Eds.; Wiley: Chichester, 1998, p. 1025, vol. 2.
3. Brooks, B. R.; Bruccoleri, R. E.; Olafson, B. D.; States, D. J.; Swaminathan, S.; Karplus, M. J Comput Chem 1983, 4, 187.
4. Catlow, C. R. A.; Dixon, M.; Mackrodt, W. C. In Computer Simulations of Solids, Lecture Notes in Physics; Catlow, C. R. A.; Mackrodt, W. C., Eds.; Springer Verlag: Berlin, 1982, p. 130, vol. 166.
5. Gao, J. In Reviews in Computational Chemistry; Lipkowitz, K. B.; Boyd, D. B., Eds.; VCH: New York, 1995, p. 119, vol. 7.
6. Gao, J. In Encyclopedia of Computational Chemistry; von Ragué Schleyer, P.; Allinger, N. L.; Kollman, P. A.; Clark, T.; Schaefer, H. F., III; Gasteiger, J.; Schreiner, P. R., Eds.; Wiley: Chichester, 1998, p. 1257, vol. 2.
7. Kömel, C. M.; Sauer, J. SOLIDS_EMBED Program Version 1.0 in Catalysis Release 3.0; BIOSYM Technologies, Inc.: San Diego, CA, 1994.
8. Elchler, U.; Kömel, C. M.; Sauer, J. J Comput Chem 1997, 18, 463.
9. Humbel, S.; Sieber, S.; Morokuma, K. J Chem Phys 1996, 105, 1959.
10. Shluger, A. L.; Gale, J. D. Phys Rev B 1996, 54, 962.
11. von Ragué Schleyer, P.; Allinger, N. L.; Clark, T.; Gasteiger, J.; Kollman, P. A.; Schaefer, H. F., III; Schreiner, P. R., Eds.; Encyclopedia of Computational Chemistry; Wiley: Chichester, 1998.
12. Froese, R. D. J.; Morokuma, K. In Encyclopedia of Computational Chemistry; von Ragué Schleyer, P.; Allinger, N. L.; Kollman, P. A.; Clark, T.; Schaefer, H. F., III; Gasteiger, J.; Schreiner, P. R., Eds.; Wiley: Chichester, 1998, p. 1244, vol. 2.
13. Merz, K. M., Jr.; Stanton, R. V. In Encyclopedia of Computational Chemistry; von Ragué Schleyer, P.; Allinger, N. L.; Kollman, P. A.; Clark, T.; Schaefer, H. F., III; Gasteiger, J.; Schreiner, P. R., Eds.; Wiley: Chichester, 1998, p. 2330, vol. 4.
14. Tomasi, J.; Pomelli, C. S. In Encylcopedia of Computational Chemistry; von Ragué Schleyer, P.; Allinger, N. L.; Kollman, P. A.; Clark, T.; Schaefer, H. F., III; Gasteiger, J.; Schreiner, P. R., Eds.; Wiley: Chichester, 1998, p. 2343, vol. 4.
15. Mordasini, T. Z.; Thiel, W. Chimia 1998, 52, 288.
16. Hillier, I. H. J Mol Struct (Theochem) 1999, 463, 45.
17. Monard, G.; Merz, K. M., Jr. Acc Chem Res 1999, 32, 904.
18. Woo, T. K.; Margl, P. M.; Deng, L.; Cavallo, L.; Ziegler, T. Catal Today 1999, 50, 479.
19. Sauer, J. Chem Rev 1989, 89, 199.
20. Zhang, Y.; Lee, T.-S.; Yang, W. J Chem Phys 1999, 110, 46.
21. Warshel, A.; Levitt, M. J Mol Biol 1976, 103, 227.
22. Gao, J.; Amara, P.; Alhambra, C.; Field, M. J. J Phys Chem A 1998, 102, 4714.
23. Philipp, D. M.; Friesner, R. A. J Comput Chem 1999, 20, 1468.
24. Bersuker, I. B.; Leong, M. K.; Boggs, J. E.; Pearlman, R. S. Int J Quantum Chem 1997, 63, 1051.
25. Pisani, C.; Dovesi, R.; Nada, R.; Kantorovich, L. N. J Chem Phys 1990, 92, 7448.
26. Pisani, C.; Corá, F.; Nada, R.; Orlando, R. Comp Phys Commun 1994, 82, 139.
27. Pisani, C.; Corá, F. Comp Phys Commun 1994, 82, 179.
28. Dixon, S. L.; Merz, K. M., Jr. J Chem Phys 1996, 104, 6643.
29. Brand, H. V.; Curtiss, L. A.; Iton, L. E. J Phys Chem 1993, 97, 12773.
30. Trout, B. L.; Chakraborty, A. K.; Bell, A. T. J Phys Chem 1996, 100, 17582.
31. Fermann, J. T.; Blanco, C.; Auerbach, S. J Chem Phys 2000, 112, 6779.
32. Noell, J. O.; Morokuma, K. J Phys Chem 1976, 80, 2675.
33. Sauer, J.; Fiedler, K.; Schirmer, W.; Zahradnik, R. In Proceedings of the 5th International Conference on Zeolites, Naples, Italy, 1980; Rees, L. C. V., Ed.; Heyden: London, 1980, p. 501.
34. Teunissen, E. H.; Jansen, A. P. J.; van Santen, R. A.; Orlando, R.; Dovesi, R. J Chem Phys 1994, 101, 5865.
35. Thompson, M. A. J Phys Chem 1996, 100, 14492.
36. Bakowies, D.; Thiel, W. J Phys Chem 1996, 100, 10580.
37. Sierka, M.; Sauer, J. Faraday Discuss 1997, 106, 41.
38. Bryce, R. A.; Buesnel, R.; Hillier, I. H.; Burton, N. A. Chem Phys Lett 1997, 279, 367.
39. Banks, J. L.; Kaminski, G. A.; Zhou, R.; Mainz, D. T.; Berne, B. J.; Friesner, R. A. J Chem Phys 1999, 110, 741.
40. Demiralp, E.; Cagin, T.; Goddard, W. A., III Phys Rev Lett 1999, 82, 1708.
41. Dapprich, S.; Komáromi, I.; Byun, K. S.; Morokuma, K.; Frisch, M. J. J Mol Struct (Theochem) 1999, 461–462, 1.
42. Maseras, F.; Morokuma, K. J Comput Chem 1995, 16, 1170.
43. Heidrich, D.; Kliesch, W.; Quapp, W. Properties of Chemically Interesting Energy Surfaces, Lecture Notes in Chemistry; Springer Verlag: Berlin, 1991, p. 78, vol. 46.

44. Carmer, C. S.; Weiner, B.; Frenklach, M. J Chem Phys 1993, 99, 1356.
45. Shoemaker, J. R.; Burggraf, L. W.; Gordon, M. S. J Phys Chem A 1999, 103, 3245.
46. Eichler, U.; Brändle, M.; Sauer, J. J Phys Chem B 1997, 101, 10035.
47. Maple, J. R.; Dinur, U.; Hagler, A. T. Proc Natl Acad Sci USA 1988, 85, 5350.
48. Maple, J. R.; Hwang, M. J.; Stockfisch, T. P.; Dinur, U.; Waldman, M.; Ewig, C. S.; Hagler, A. T. J Comput Chem 1994, 15, 162.
49. Jackson, R. A.; Catlow, C. R. A. Mol Simul 1988, 1, 207.
50. Sanders, M. J.; Leslie, M.; Catlow, C. R. A. J Chem Soc Chem Commun 1984, 1271.
51. Hill, J.-R.; Sauer, J. J Phys Chem 1994, 98, 1238.
52. Hill, J.-R.; Sauer, J. J Phys Chem 1995, 99, 9536.
53. Sauer, J.; Schröder, K.-P.; Temath, V. Coll Czech Chem Commun 1998, 63, 1394.
54. Nachtigallová, D.; Nachtigall, P.; Sierka, M.; Sauer, J. Phys Chem Chem Phys 1999, 1, 2019.
55. Schröder, K.-P.; Sauer, J. J Phys Chem 1996, 100, 11043.
56. Sierka, M.; Sauer, J. J Chem Phys 2000, 112, 6983.
57. Ricchiardi, G.; de Man, A. J. M.; Sauer, J. Phys Chem Chem Phys 2000, 2, 2195.
58. Sauer, J. In Encyclopedia of Computational Chemistry; von Ragué Schleyer, P.; Allinger, N. L.; Clark, T.; Gasteiger, J.; Kollman, P. A.; Schaefer, H. F., III; Schreiner, P. R., Eds.; Wiley: Chichester, 1998, p. 3248, vol. 5.
59. Hill, J.-R.; Freeman, C. M.; Subramanian, L. In Reviews in Computational Chemistry; Lipkowitz, K. B.; Boyd, D. B., Eds.; VCH: New York, 2000, p. 141, vol. 16.
60. Demontis, P.; Suffritti, G. B. Chem Rev 1997, 97, 2845.
61. Leslie, M. Physica 1985, 131B, 145.
62. Dick, B. G., Jr.; Overhauser, A. W. Phys Rev 1958, 112, 90.
63. Brändle, M.; Sauer, J. J Mol Catal A 1997, 119, 19.
64. Warshel, A. Computer Modeling of Chemical Reactions in Enyzmes and Solutions; Wiley: New York, 1991.
65. Åqvist, J.; Warshel, A. Chem Rev 1993, 93, 2523.
66. Sauer, J.; Sierka, M.; Haase, F. In Transition State Modeling for Catalysis; ACS Symposium Series 721; Truhlar, D. G.; Morokuma, K., Eds.; American Chemical Society: Washington, DC, 1999, p. 358.
67. Chang, Y.-T.; Miller, W. H. J Phys Chem 1990, 94, 5884.
68. Kim, Y.; Corchado, J. C.; Villa, J.; Xing, J.; Truhlar, D. G. J Chem Phys 2000, 112, 2718.
69. Kömel, C. M.; Sauer, J. QuantMM Module Catalysis Software, Release 3.0.0; BIOSYM/MSI: San Diego, CA, 1995.
70. Ahlrichs, R.; Bär, M.; Häser, M.; Horn, H.; Kölmel, C. Chem Phys Lett 1989, 162, 165.
71. Ahlrichs, R.; Elliott, S. D.; Huniar, U. Ber Bunsenges Phys Chem 1998, 102, 795.
72. Frisch, M. J.; Trucks, G. W.; Schlegel, H. B.; Scuseria, G. E.; Robb, M. A.; Cheeseman, J. R.; Zakrzewski, V. G.; Montgomery, J. A., Jr.; Stratmann, R. E.; Burant, J. C.; Dapprich, S.; Millam, J. M.; Daniels, A. D.; Kudin, K. N.; Strain, M. C.; Farkas, O.; Tomasi, J.; Barone, V.; Cossi, M.; Cammi, R.; Mennucci, B.; Pomelli, C.; Adamo, C.; Clifford, S.; Ochterski, J.; Petersson, G. A.; Ayala, P. Y.; Cui, Q.; Morokuma, K.; Malick, D. K.; Rabuck, A. D.; Raghavachari, K.; Foresman, J. B.; Cioslowski, J.; Ortiz, J. V.; Stefanov, B. B.; Liu, G.; Liashenko, A.; Piskorz, P.; Komaromi, I.; Gomperts, R.; Martin, R. L.; Fox, D. J.; Keith, T.; Al-Laham, M. A.; Peng, C. Y.; Nanayakkara, A.; Gonzalez, C.; Challacombe, M.; Gill, P. M. W.; Johnson, B.; Chen, W.; Wong, M. W.; Andres, J. L.; Head–Gordon, M.; Replogle, E. S.; Pople, J. A. Gaussian 98, Revision A.3; Gaussian, Inc.: Pittsburgh, PA, 1998.
73. DMol^3 3.5; Molecular Simulations, Inc.: San Diego, CA, 1997.
74. DISCOVER; Molecular Simulations, Inc.: San Diego, CA, 1998.
75. OPEN FORCE FIELD; Molecular Simulations, Inc.: San Diego, CA, 1998.
76. Gale, J. D. J Chem Soc Faraday Trans 1997, 93, 629; Program GULP (General Utility Lattice Program); Royal Institution/Imperial College: London, 1992–1994.
77. Helgaker, T. Chem Phys Lett 1991, 182, 503.
78. Culot, P.; Dive, G.; Nguyen, V. H.; Ghuysen, J. M. Theoret Chim Acta 1992, 82, 189.
79. Fletcher, R. Practical Methods of Optimization; John Wiley & Sons, Inc.: New York, 1987.
80. Baker, J. J Comput Chem 1986, 7, 385.
81. Zhang, Y.; Liu, H.; Yang, W. J Chem Phys 2000, 112, 3483.
82. Sierka, M.; Sauer, J. J Am Chem Soc, submitted.
83. Meier, W. M.; Olson, D. H. Atlas of Zeolite Structure Types; Butterworth–Heinemann: London, 1992; http://www.iza-sc.ethz.ch/IZA-SC/Atlas/AtlasHome.html.
84. Lamberti, C.; Bordiga, S.; Salvalaggio, M.; Spoto, G.; Zecchina, A.; Geobaldo, F.; Vlaic, G.; Bellatreccia, M. J Phys Chem B 1997, 101, 344.
85. Nachtigall, P.; Nachtigallová, D.; Sauer, J. J Phys Chem B 2000, 104, 1738.
86. Nachtigall, P.; Nachtigallová, D.; Sauer, J., in preparation.
87. Rodriguez-Santiago, L.; Sierka, M.; Branchadell, V.; Sodupe, M.; Sauer, J. J Am Chem Soc 1998, 120, 1545.
88. Schneider, W. F.; Hass, K. C.; Ramprasad, R.; Adams, J. B. J Phys Chem B 1997, 101, 4353.
89. Schneider, W. F.; Hass, K. C.; Ramprasad, R.; Adams, J. B. J Phys Chem B 1998, 102, 3692.
90. Tajima, N.; Hashimoto, M.; Toyama, F.; El-Nahas, A. M.; Hirao, K. Phys Chem Chem Phys 1999, 1, 3823.
91. Brändle, M.; Sauer, J. J Am Chem Soc 1998, 120, 1556.
92. Sierka, M.; Eichler, U.; Datka, J.; Sauer, J. J Phys Chem B 1998, 102, 6397.
93. Sauer, J. In Modeling of Structure and Reactivity in Zeolites; Catlow, C. R. A., Ed.; Academic Press: London, 1992, p. 183.
94. Sauer, J.; Eichler, U.; Meier, U.; Schäfer, A.; von Arnim, M.; Ahlrichs, R. Chem Phys Lett 1999, 308, 147.
95. Brand, H. V.; Curtiss, L. A.; Iton, L. E. J Phys Chem 1992, 96, 7725.
96. Sauer, J.; Ugliengo, P.; Garrone, E.; Saunders, V. R. Chem Rev 1994, 94, 2095.
97. Greatbanks, S. P.; Sherwood, P.; Hillier, I. H.; Hall, R. J.; Burton, N. A.; Gould, I. R. Chem Phys Lett 1995, 234, 367.
98. de Vries, A. H.; Sherwood, P.; Collins, S. J.; Rigby, A. M.; Rigutto, M.; Kramer, G. J. J Phys Chem B 1999, 103, 6133.

99. Brändle, M.; Sauer, J.; Dovesi, R.; Harrison, N. M. J Chem Phys 1998, 109, 10379.
100. Maiti, A.; Sierka, M.; Andzelm, J.; Golab, J.; Sauer, J. J Phys Chem A, submitted.
101. Lopez, N.; Pacchioni, G.; Maseras, F.; Illas, F. Chem Phys Lett 1998, 294, 611.
102. Choi, C. H.; Gordon, M. S. J Am Chem Soc 1999, 121, 11311.
103. Frenklach, M.; Skokov, S.; Weiner, B. Nature 1994, 372, 535.
104. Skokov, S.; Weiner, B.; Frenklach, M. Phys Rev B 1994, 49, 11374.
105. Skokov, S.; Carmer, C. S.; Weiner, B.; Frenklach, M. Phys Rev B 1994, 49, 5662.
106. Skokov, S.; Weiner, B.; Frenklach, M. J Phys Chem 1994, 98, 7073.
107. Skokov, S.; Weiner, B.; Frenklach, M. J Phys Chem 1994, 98, 8.
108. Sinclair, P. E.; de Vries, A.; Sherwood, P.; Catlow, C. R. A.; van Santen, R. A. J Chem Soc Faraday Trans 1998, 94, 3401.
109. Nicholas, J. B.; Trouw, F. R.; Mertz, J. E.; Iton, L. E.; Hopfinger, A. J. J Phys Chem 1993, 97, 4149.
110. Shluger, A. L.; Kantorovich, L. N.; Livshits, A. I.; Gillan, M. J. Phys Rev B 1997, 56, 15332.